The American Journal of Pathology, Vol. 169, No. 2, August 2006

DOI: 10.2353/ajpath.2006.060002

Neurobiology

Alzheimer's Disease-Like Tau Neuropathology Leads to Memory Deficits and Loss of Functional Synapses in a Novel Mutated Tau Transgenic Mouse without Any Motor Deficits

Katharina Schindowski,*† Alexis Bretteville,*† Karelle Leroy,‡ Séverine Bégard,*† Jean-Pierre Brion,‡ Malika Hamdane,*† and Luc Buée*†

From INSERM U815, Lille, France; the Faculté de Médecine,† Institut de Médecine Prédictive et Recherche Thérapeutique, Université Lille 2, Lille, France; and the Laboratory of Histology and Neuropathology,‡ Free University of Brussels, School of Medicine, Brussels, Belgium*

Tau transgenic mice are valuable models to investigate the role of tau protein in Alzheimer's disease and other tauopathies. However, motor dysfunction and dystonic posture interfering with behavioral testing are the most common undesirable effects of tau transgenic mice. Therefore, we have generated a novel mouse model (THY-Tau22) that expresses human 4-repeat tau mutated at sites G272V and P301S under a Thy1.2-promotor, displaying tau pathology in the absence of any motor dysfunction. THY-Tau22 shows hyperphosphorylation of tau on several Alzheimer's disease-relevant tau epitopes (AT8, AT100, AT180, AT270, 12E8, taupSer396, and AP422), neurofibrillary tangle-like inclusions (Gallyas and MC1-positive) with rare ghost tangles and PHF-like filaments, as well as mild astrogliosis. These mice also display deficits in hippocampal synaptic transmission and impaired behavior characterized by increased anxiety, delayed learning from 3 months, and reduced spatial memory at 10 months. There are no signs of motor deficits or changes in motor activity at any age investigated. This mouse model therefore displays the main features of tau pathology and several of the pathophysiological disturbances observed during neurofibrillary degeneration. This model will serve as an experimental tool in future studies to investigate mechanisms underlying cognitive deficits during pathogenic tau aggregation. ***(Am J Pathol 2006, 169:599–616; DOI: 10.2353/ajpath.2006.060002)***

Alzheimer's disease (AD) is the most common form of dementia in the elderly and is characterized neuropathologically by the presence of intracellular neurofibrillary tangles (NFTs) and senile plaques in the brain and by a major loss of synaptic connections. NFTs are neuronal inclusions of the microtubule-associated tau protein and are composed of aggregated phosphorylated tau. In AD, NFTs occur in the hippocampus, the entorhinal and polymodal association cortices, and in the basal forebrain. These brain areas are also severely affected by neuronal and synaptic loss. The loss of neurites, synapses, and neurons represent one of the reasons for the cognitive deficits and dementia of AD.[1–4]

In addition to the neuropathological hallmarks of AD, there are also a number of other pathophysiological disturbances that are observed in AD brain including the inflammatory reaction of glial cells (gliosis).[5] It is now increasingly recognized that synaptic dysfunction is a major pathophysiological feature of AD. It has been suggested that disruption of neuronal communication is an early event in the disease progression and could occur independently of neuronal loss per se.[6]

Supported by the Centre National de la Recherche Scientifique; the Fédération pour la Recherche sur le Cerveau; Gis-Longévité; the Institut National de la Santé et de la Recherche Médicale; the European Community (an integrated project for abnormal proteins in the pathogenesis of neurodegenerative diseases, LSHM-CT-2003-503330 and a Marie Curie Fellowship K.S.); the Association d'Etudes et de Recherche sur la Maladie d'Alzheimer; the International Alzheimer Research Foundation (to J.P.B.); and the Région Nord/Pas-de-Calais and Centre Hospitalier Régional Universitaire-Lille (scholarship to A.B.).

A.B. and K.L. contributed equally to this study.

Accepted for publication April 27, 2006.

Mice for this study were generated in collaboration with Günter Tremp and Nathalie Touchet from Sanofi-Aventis, Vitry-sur-Seine, France.

Supplemental material for this article can be found on *http://ajp.amjpathol.org.*

Address reprint requests to Katharina Schindowski, INSERM U815, Place de Verdun, 59045 Lille Cedex, France. E-mail: katharina.schindowski@lille.inserm.fr.

Table 1. Antibodies and Lectin Used in This Study

Antibody	Species	Specificity	Dilution	Source
AT8	Mouse	Tau; pSer202/pThr205	1:400 (WB); 1:10,000 (ICH/IF)	Innogenetics (Gent, Belgium)
pSer396	Rabbit	Tau; pSer396	1:5000	Biosource (Camarillo, CA)
AT180	Mouse	Tau; pThr231	1:500	Innogenetics
AT270	Mouse	Tau; pThr181	1:4000 (WB); 1:2000 (IHC)	Innogenetics
AP422/988	Mouse	Tau; pSer422	1:5000	Bussiere et al[61]
AT100	Mouse	Tau; pThr212/pSer214	1:1000 (WB); 1:2000 (IHC)	Innogenetics
M19G	Rabbit	Tau; human-specific, 1 to 19 amino acids	1:20,000	Bussiere et al[61]
MC1	Mouse	Tau; conformational epitope, 7 to 9 and 326 to 330 amino acids	1:1000	P. Davies
PHF-1	Mouse	Tau; pSer396/pSer404	1:50,000	P. Davies
Tau-5	Mouse	Tau; human/mouse-specific	1:10,000	Biosource
TP20	Rabbit	Tau; human-specific, 33 to 41 amino acids	1:2000	Brion et al[15]
12E8	Mouse	Tau; pSer262	1:400	Seubert et al[62]
GFAP	Rabbit	GFAP	1:20,000 (IF)	DAKO (Trappes, France)
Synaptophysin	Rabbit	Synaptophysin	1:1000	Santa Cruz Biotechnology (Santa Cruz, CA)
Synaptotagmin	Rabbit	Synaptotagmin I	1:1000	Synaptic System (Göttingen, Germany)

Lectin	Specificity	Dilution	Source
Biotinylated tomato lectin (*Lycopersicon esculentum*)	Microglia	6 μg/ml	Sigma-Aldrich L-0651 (Sigma-Aldrich, Lyon, France)

Tau transgenic (Tg) and gene-targeted mice are valuable models that reproduce various aspects of tauopathies and AD tau pathology with associated cognitive changes. Several models with single tau mutations, including P301L,[7–9] P301S,[10] G272V,[11] V337M,[12] and R406W,[13,14] or overexpression of human tau isoforms[15–17] have been generated. However, none of these mouse models fully recapitulates the neuropathological spectrum of tangle pathology observed in AD. Moreover, most published models show motor deficits and hind limb paralysis with increasing pathology caused by tau expression in the spinal cord. Motor dysfunction makes it very difficult to study these animals with behavioral experiments or in the late stages of tau pathology because they usually die earlier. Therefore, our aim was to generate a new tau mouse model without APP pathology that does not display any motor dysfunction to investigate the pure pathogenic tau accumulation and its effects in AD tau pathology. In the present study, we describe the construction and characterization of a mouse model expressing double-mutated human tau that displays several of the key features of tau pathology and other pathological changes, such as loss of synaptic function and impaired behavior, observed in AD and other types of tauopathies.

Materials and Methods

Generation of Tg Mice Expressing G272V and P301S Human Tau

The cDNA of the 412 amino acid 4-repeat isoform of human tau (htau 46, cloned from human brain cDNA) was a kind gift from M. Goedert (Medical Research Council Laboratory of Molecular Biology, Cambridge, UK).[18] To introduce a Kozak-sequence and *Xho*I site, the cDNA was reamplified with the following primers: Tau5′tg 5′-CTCGAGGATGGCTGAGCCCCGCCAGG-3′ and Tau3′tg 5′-CTCGAGTCACAAACCCTGCTTGGCCAGGGAGG-3′ and mutated at G272V and P301S (numbering according to the longest human tau isoform) by polymerase chain reaction (PCR)-based site-directed mutagenesis (Stratagene, Amsterdam, The Netherlands). This cDNA-construct was inserted into the *Xho*I-sites of a Thy1.2 expression vector.[19,20] The Thy1.2 promotor specifically drives expression in neurons[19] that starts at postnatal day 6[21] and therefore does not directly affect embryonic development. The vector was then microinjected into a C57BL6/CBA background and backcrossed to C57BL6 for more than five generations. Tg mice were screened for the Tau transgene by PCR analysis of DNA prepared from tail biopsies (DNeasy tissues kit; Qiagen, Courtaboeuf, France). The forward (5′-ATGGCTGAGCCCCGCCAGGAG-3′) and the reverse (5′-TGGAGGTTCACCAGAGCTGGG-3′) primers were used to amplify a 250-bp fragment of Tau DNA. The number of integrated copies was determined by Southern blot analysis.

All Tg mice used in the present study were heterozygous. Non-Tg littermates were used as wild-type (WT) controls for all experiments. The chosen line (THY-Tau22) is fertile with normal frequency and size of litters and stably transmits the transgene to its offspring. All experiments on animals were performed in compliance with, and following the approval of, the Centre National de la Recherche Scientifique–Institute of Laboratory Animal

Resources Committee, in accordance with standards for the care and use of laboratory animals and with French and European Community rules.

Western Blot Analysis

Whole brains were dissected by separating the cortex from the hippocampus and thalamus. Cortical and hippocampal preparations were homogenized in cell-lysis buffer (Cell Signaling Technology, Danvers, MA) using several strokes of sonification and then boiled at 100°C for 10 minutes. For Western analysis, 10 or 25 μg of total protein were resolved on sodium dodecyl sulfate-polyacrylamide gel electrophoresis, blotted onto nitrocellulose or polyvinylidene difluoride membranes (all from Invitrogen), incubated with appropriate antibodies (Table 1), and developed using the ECL chemiluminescence kit (Amersham/GE Healthcare, Orsay, France). Protein levels were visualized and quantified using an imaging system (LAS-3000 2.0; Fuji Photo Film Co. Ltd.). Human brain samples were from the Association d'Etudes et de Recherche sur la Maladie d'Alzheimer brain bank.[22]

Histology

Immunohistochemistry and Immunofluorescence

Tg and WT mice from 3 to 17 months were anesthetized and transcardially perfused sequentially with 0.9% NaCl and 4% paraformaldehyde in 0.1 mol/L phosphate-buffered saline (PBS) (pH 7.4) or 10% formalin and 4% paraformaldehyde in 0.1 mol/L PBS (pH 7.4). Brains and spinal cords were removed and stored in 4% paraformaldehyde. Some samples were embedded in paraffin and cut on a sliding microtome at a thickness of 10 μm. Cryosections (14 μm) were cut on a cryostat and mounted on chrome alum-coated slides. Endogenous peroxidase was quenched by treating the section with methanol containing 0.3% H_2O_2 for 30 minutes. Sections were blocked in 10% horse serum. Primary antibodies were used according to Table 1 and incubated overnight at 4°C in the presence of 1% horse serum. All secondary biotinylated or fluorescein-, Texas Red-, and AMCA-coupled antibodies, fluorochromes, ABC-kit, and 3,3′-diaminobenzidine as chromogen for peroxidase activity were from Vector Laboratories, Burlingame, CA. Incubation with the secondary antibody was done at room temperature for 1 hour. All washing steps (3 × 10 minutes) and antibody dilution were done using phosphate-buffered saline (0.1 mol/L PBS, pH 7.4) or Tris-buffered saline (0.01 mol/L Tris, 0.15 mol/L NaCl, pH 7.4). Incubation with the ABC complex and detection with 3,3′-diaminobenzidine was done according to the manufacturer's manual. Hematoxylin counterstaining was performed according to standard procedures. A minimum of three mice per genotype, age, and sex was used for each determination. Data were analyzed by analysis of variance with Bonferroni's post test.

Gallyas Silver Impregnation

Floating cryosections (14 μm) were silver stained according to Braak and Braak.[23]

4′,6-Diamidino-2-Phenylindole (DAPI) Staining

Cryosections were mounted in VectaShield containing DAPI (Vector Laboratories).

Nissl/Cresylviolet Staining

Mounted cryosections (14 μm) were rinsed 5 minutes in distilled water and transferred to a 1.5% cresyl-violet solution. Sections were then incubated in a solution containing 1% glacial acetic acid and 16% ethanol in distilled water. Sections were then transferred to an ascending alcohol series (70%, 90%, 96%, and 99% ethanol), and finally to toluene, before they were coverslipped using VectaMount (Vector Laboratories).

Semiquantitative Estimation of Cell Density

Images were made using a software-controlled (Leica FW 4000; Leica, Rueil-Malmaison, France) digital camera (Leica DC 300FX) attached to a microscope (Leica DM RB), stored onto hard disk, and analyzed offline. For analysis, images were taken using a ×40 objective. In each image, stained cells were counted in a counting frame.

Transmission Electron Microscopy

Tg and WT mice were anesthetized with chloral hydrate and perfused intracardially with a solution of 2% (w/v) paraformaldehyde and 2% (v/v) glutaraldehyde in 0.1 mol/L phosphate buffer at pH 7.4.[15] Tissue blocks were quickly dissected and further fixed by immersion with 4% (w/v) glutaraldehyde in 0.1 mol/L phosphate buffer at pH 7.4 for 90 minutes. After washing in Millonig's buffer with 0.5% (w/v) sucrose for 24 hours, the tissue sections were postfixed in 2% (w/v) OsO_4 for 30 minutes, dehydrated, and embedded in Epon. Semithin sections were stained with toluidine blue. Ultrathin sections were counterstained with uranyl acetate and lead citrate and observed with a Zeiss EM 809 transmission electron microscope at 80 kV. Measurements of the diameter of filaments were performed on digitalized images using the public domain NIH ImageJ program and given in mean ± SD.

Electrophysiological Recordings

Hippocampal slices (400 μm thick) were prepared from male tau Tgs and WT controls at 6 to 7 and 14 to 15 months of age. Slices were cut transversally on a McIlwain tissue chopper (Campden Instruments, Loughborough, UK) and placed in a submersion-type recording chamber through which artificial cerebrospinal fluid (ACSF: 124 mmol/L NaCl, 3 mmol/L KCl, 1.25 mmol/L NaH_2PO_4, 1.3 mmol/L $MgSO_4$, 2 mmol/L $CaCl_2$, 26 mmol/L $NaHCO_3$, and 10 mmol/L glucose) was continu-

ously superfused at 2.5 to 3 ml/minute. The ACSF was bubbled with a mixture of 95% O_2 and 5% CO_2 and maintained at 30°C. Test stimulations (0.1 ms in duration) were delivered at constant intensity every 30 seconds through bipolar stainless steel electrodes placed in the stratum radiatum of the CA1 area. Extracellular field excitatory postsynaptic potentials (EPSPs) were recorded with a monopolar tungsten electrode implanted in the same region. To analyze synaptic transmission efficiency, input/output plots were constructed individually for each slice by applying single stimuli in increments of 20 μA from 100 μA (threshold) to 300 μA. To evaluate synaptic plasticity, a 30-minute baseline was recorded with the stimulation intensity set at half-maximal strength. Long-term potentiation (LTP) was induced by applying a single train of tetanic stimulation at a frequency of 100 Hz for 1 second, after which the size of the EPSP was monitored for 90 minutes.

Behavioral Tests

Modified Irwin Examination

A comprehensive screen, modified from Irwin,[24] was used to determine whether any of the mice exhibited physiological, behavioral, or sensorimotor impairments related to their genotype. To explore motor skills, coordination, and muscle strength, the mice were placed on a wire that was tightened between two 30-cm-high columns and their ability to balance on the wire was assessed. In addition, their ability to grasp and hang on the wire with all four paws for at least 5 seconds and to climb back on the wire was determined.

Rotarod Test

Motor coordination and balance were tested using an accelerating rotarod (Rota-ROD LE 8200, Bioseb, Chaville, France). The mice were allowed to explore the rotarod for 2 minutes without rotation and then the drum was slowly accelerated to 14 rotations per minute (rpm). The mice were subjected to 2-minute training trials twice a day for 2 consecutive days. On day 3 the rotarod test was performed by placing the mice on the rotating drum (25 rpm) for 2 minutes and the time each animal was able to maintain its balance walking on top of the rod was measured. Data were analyzed by Student's *t*-test.

Elevated Plus Maze

The elevated plus maze is a test of anxiety and motor behavior. The maze was set at a height of 65 cm and consisted of four white Plexiglas arms, each 6 cm wide and 28 cm long with 10-cm-high gray walls surrounding the two enclosed arms. Individual mice were placed in the center of the maze facing an open arm and the total distance and time spent in each arm was measured by a video camera connected to a computer and analyzed with the Videotrack Software (View Point S.A., Champagne au Mont d'Or, France). The total time spent in open and closed arms, the number of arm entries, and the inactive time were calculated. Data were analyzed by unpaired Student's *t*-tests.

Spatial Learning and Memory in the Morris Water Maze (MWM)

This experiment was performed in a circular pool, 90 cm in diameter, made of white plastic and filled with milky colored water. An escape platform, 8 cm in diameter, made of clear plastic was submerged 0.5 cm under the water level. Visual clues were provided by different geometrical forms printed in A4-sized letters and placed on the four surrounding walls (distance from the pool was ~50 to 70 cm). Each mouse was given four trials daily (5- to 7-minute interval between trials, a total of 16 trials) for 4 days. Each trial was performed from one of four different starting points. The movement of the mice was monitored using Videotrack Software (View Point). The time taken to locate the escape platform (escape latency; up to 60 seconds) was determined. After locating the platform the mouse was allowed to sit on it for 15 seconds. Mice who failed to find the platform within 60 seconds were guided to it and allowed to stay on it for 15 seconds. A latency of 60 seconds was entered into the record for such an occurrence. All four trials per day were averaged for statistical analysis, except for the first trial on day 1. On day 9 (5 days after the last training) mice were subjected to a 60-second probe trial in which the platform was removed and the mice were allowed to search for it. The time that each animal spent in each quadrant was recorded (quadrant search time). Four groups of male mice were used at 2 to 3, 7, 10, and 14 months. The 7-month-old Tg and WT mice showed severe freezing behavior (eg, lying motionless in the water and refusing to swim) that strongly interfered with the test and were excluded from the data analysis. All behavioral tests were conducted under a quiet and light-reduced environment. Data were analyzed by Student's *t*-tests.

Results

Generation and Selection of THY-Tau Tg Mice

The tau mutations G272V and P301S were generated by site-directed mutagenesis PCR into the human 4-repeat tau cDNA and subcloned into the Thy1.2-expression vector (Figure 1A). After microinjection and implantation, eight viable THY-Tau mouse lines were obtained. A variable number of DNA copies were detected in each of the lines from 1 copy up to 10 copies (Figure 1B). Human tau protein expression in the heterozygous animals from all lines was analyzed in the cortex, hippocampus-enriched fractions, and spinal cord. Five lines expressed low levels of human tau in mouse brain and were excluded. One important aim of this study was to generate a tau Tg mouse line with tau pathology similar to that observed in AD in the absence of any motor dysfunction. Therefore, expression of tau protein in the spinal cord, accompanied by motor deficits and paralysis, was an exclusion criterion for each line. Because

A

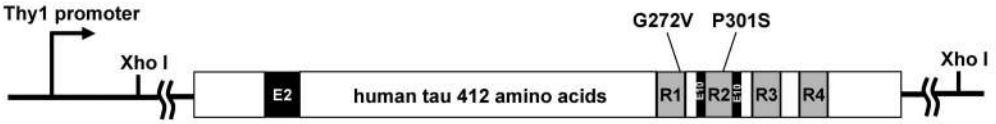

B

mouse line	copy-number	htau in cortex		htau in hippocampus		htau in spinal cord	
		3 months	12 months	3 months	12 months	3 months	12 months
22	10	+++	++++	++	+++	(+)	+
30	5-10	+++	++++	+++	++++	++	+++
52	1	(+)	++	(+)	++	(+)	(+)

C

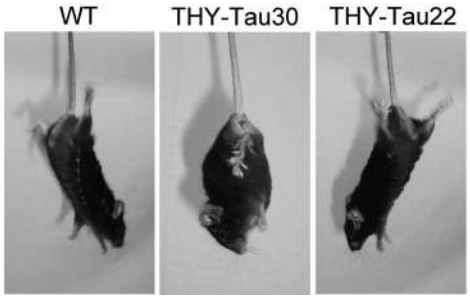

D

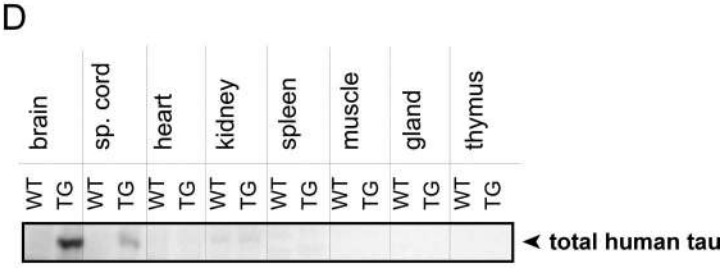

Figure 1. Generation of the THY-Tau Tg mouse model. **A:** The human 412 amino acid double-mutated *tau* construct used for microinjection. Exons 2 and 10 are depicted by black boxes and microtubule binding repeats by gray-shaded boxes. The human 4-repeat *tau* was site-directed mutated at G272V and P301S and cloned as *Xho*I-fragment into a Thy1.2-expression vector. **B:** THY-Tau mouse lines, transgene DNA copy number, and relative protein levels of total human tau in cortex, hippocampus, and spinal cord compared to endogenous tau in WTs from three adult animals at 3 and 12 months: (+), traces; +, low levels (similar to endogenous tau); ++, medium levels (twofold to threefold greater than endogenous tau); +++, high levels (fourfold to fivefold greater than endogenous tau); ++++, very high levels (fivefold to sixfold greater than endogenous tau; detection with M19G and tau-5). **C:** Positive grasping reflex in response to tail hang in a 10-month-old tau Tg mouse of line 30 (THY-Tau30) with hind limb paralysis. Mice from line 22 (THY-Tau22) and WTs at the same age do not display this reflex. **D:** Expression of the transgene in different tissues from THY-Tau22. Immunoreactivity for tau-5 (total tau) is only found in the brain and minor traces in spinal cord. Representative immunoblot from a 6-month-old male THY-Tau22 (Tg) and WT.

mice from line 30 show rather high levels of human tau in spinal cord and starting by the age of 7 to 8 months they display dystonic posture and paralyzed hind limbs (Figure 1, B and C), the line was excluded. Nevertheless, the tau profile in the brain of line 30 is still quite interesting with high levels in hippocampus and rather low levels in the cortex. The tau pathology of line 30 is currently under investigation. Line 52 expresses low levels of the tau construct in hippocampus and cortex and develops tau accumulation at more than 18 months of age. Homozygous animals of line 52 are viable and their characterization is also currently being investigated.

By contrast, line 22 showed high levels of human tau protein in brain homogenates, only minor traces in the spinal cord (Figure 1D), and no dystonic hind limbs (Figure 1C) in all ages investigated (up to 18 months) and was therefore chosen as the line for further characterization in this study. Several tissues from line 22 were analyzed for expression of human tau ~65 kd by immunoblotting. No Tg tau was found in other organs (Figure 1D), even after long overexposure (data not shown). All animals characterized in this study derived from line 22 are heterozygous and are named THY-Tau22. During this study two females (5 to 7 months old) and three males (17 months old) died, representing an overall mortality of 3% in THY-Tau22 mice. No mortality was observed in the littermate WT controls. The Tg mice had a reduced bodyweight compared to their WT littermates by ~15% (THY-Tau22, 22.87 ± 0.47 g; WT, 26.95 ± 0.44 g, $n = 8$ males per group, 2 months old, $^{***}P < 0.001$; THY-Tau22, 28.25 ± 0.53 g; WT, 34.76 ± 1.25 g, $n = 8$ males per group, 7 months old, $^{***}P < 0.001$; THY-Tau22, 27.42 ± 1.43 g; WT, 32.47 ± 0.76 g, $n = 8$ males per group, 14 months old, $^{**}P < 0.01$). This effect was similar in females.

AD-Relevant Pathological Tau Hyperphosphorylation and Conformation in THY-Tau22 Mice

Under normal physiological conditions tau is a highly soluble protein that becomes insoluble by conformational changes and pathological phosphorylation in AD and in frontotemporal dementia with parkinsonism linked to chromosome 17 (FTDP-17). The result is a translocation of the insoluble tau species from the axon, accumulation in the cell bodies, and formation of NFT.

Sections of THY-Tau22 mouse brain and homogenates from dissected cortices were screened with a battery of

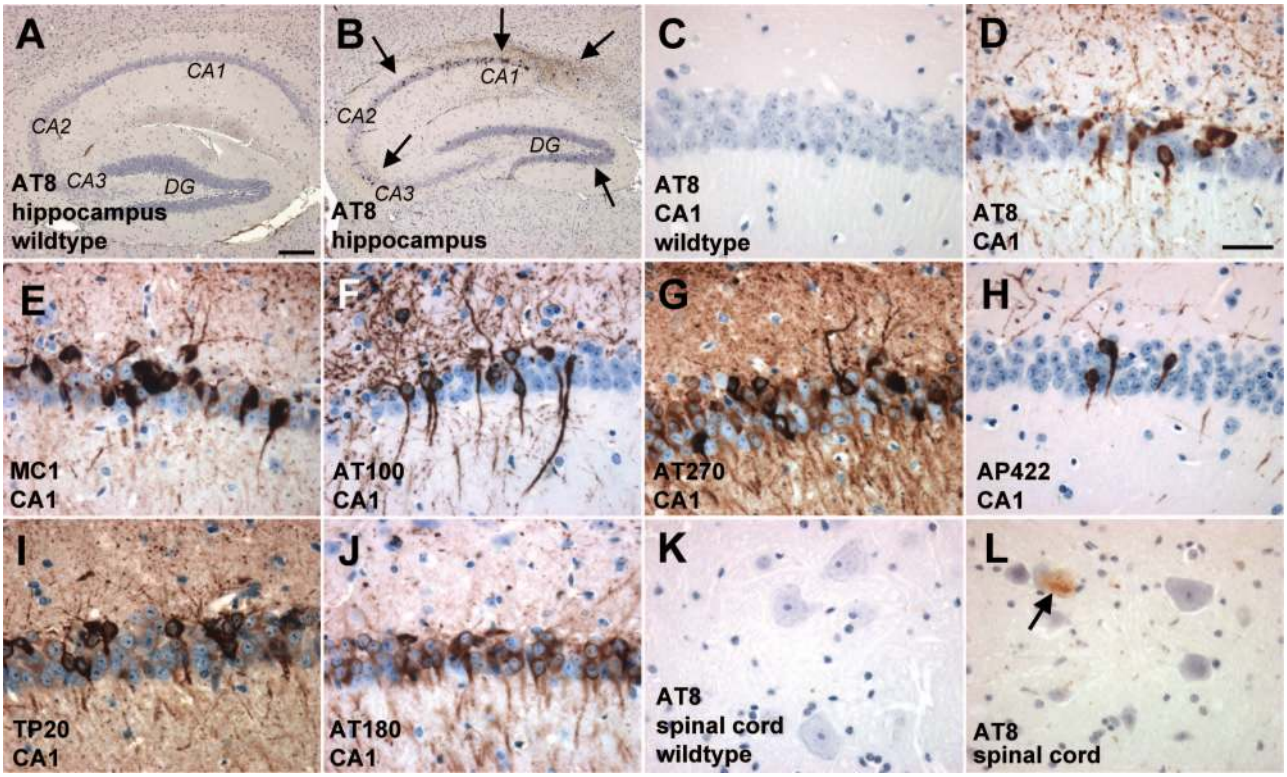

Figure 2. Accumulation of pathological tau species in THY-Tau22. Immunohistochemical studies revealed the accumulation of abnormal tau conformation and phosphorylation in 12-month-old THY-Tau22 compared to non-Tg WTs in hippocampus (**A** and **B**, note the **arrows** pointing to the most representative dots in the Tg), CA1 sector (**C–J**), and spinal cord (**K** and **L**, note the **arrow**). Hyperphosphorylation was identified as brown color and detected with AT8 (**A–D** and **K–L**), AT100 (**F**), AT270 (**G**), AP422/988 (**H**), human-specific TP20 tau antibody (**I**), AT180 (**J**), and abnormal tau conformation with MC1 (**E**). No positive labeling was observed after parallel processing of littermate WT tissue (**A** and **C**, 12 months old). Representative sections are shown of 10 animals used at the age indicated. Scale bars: 200 μm (**A**, **B**); 25 μm (**C–L**).

phospho-specific antibodies (Figures 2 and Figure 4 and Supplementary Figure S1 at *http://ajp.amjpathol.org*). Phosphorylation of tau was present from the age of 3 months (AT8 and AT270) and 6 months (PHF-1, AT100, AT180, and AP422/988; Figure 4A) and abnormal conformational changes of tau using MC1 antibody by 3 months (data not shown). Abnormal tau species were detected in neocortex, the hippocampus—starting early and being very prominent in the CA1 pyramidal layer (Figure 2, C–J) and spreads later to the dentate gyrus (DG) and CA3 subfield —the striatum, the olfactory bulb, the occipital cortex, the amygdala, the ventral thalamic nuclei, and deep layers of the entorhinal cortex (Supplementary Figure S1 at *http://ajp.amjpathol.org*). The number of neurons containing pathological tau species significantly increased with age (demonstrated by PHF-1 immunoreactivity and Gallyas silver stain in Figure 3). Even in 12-month-old THY-Tau22 mice, only a few phospho-tau-positive cells were detected in the spinal cord (Figure 2L) and in the deep cerebellar nuclei (data not shown). Before abnormal tau species became detectable in neuronal cell bodies they were earlier observed in axonal tracts and neurites (eg, the mossy fibers in the hippocampus; data not shown). In older mice labeling was associated with well-defined intracellular inclusions in neuronal perikarya and in proximal portions of dendrites (Figures 2 and 3), indicating that phosphorylated tau was translocated to the cell bodies.

Older mice at 12 months showed the full AD-like spectrum of tau pathology including tau hyperphosphorylation and pathological tau phosphorylation (Figures 2 and 4), formation of NFT-like Gallyas silver-positive inclusions (Figure 3), tau filaments (Figure 5), and ghost tangles (Figure 6, F–G). However, a minor reduction in the number and size of AT8-positive neurons in aged THY-Tau22 in cell bodies in the frontal cortex, the CA1 and CA3 region, and in neurites and fiber tracts of the whole hippocampus was observed (data not shown). All stainings were similar between genders with a very small tendency in males toward increased tau pathology and highly consistent when mice of the same age were compared. None of the antibodies used showed any immunoreactivity in non-Tg animals in immunohistochemistry (Figure 2, A and C). There was no staining of glial cells with any of these antibodies.

Homogenates of frontal cortex from 3- to 14-month-old mice were analyzed by immunoblotting. In general, tau proteins separated as a complex set of bands reflecting the expression of differentially phosphorylated isoforms (Figure 4A). Immunoblotting of total human tau with M19G revealed a 64-kd band that was present at 3 months and increased with age and a 69-kd-band that appeared at 6 to 10 months and increased with age, representing the hyperphosphorylated and abnormal phosphorylated variants of the Tg isoform. AD-like hyperphosphorylation of Thr181 (AT270) and Ser396 was de-

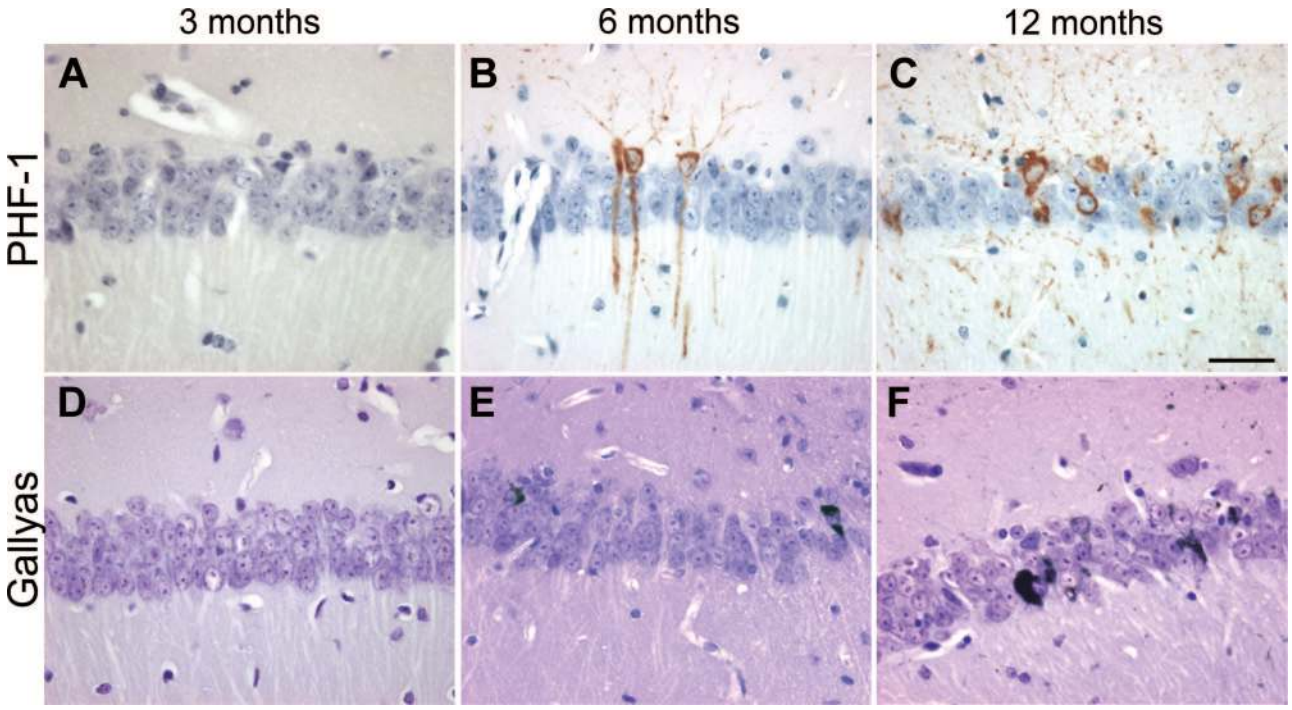

Figure 3. Age kinetics of neurofibrillary inclusions and tau accumulation in THY-Tau22 mice. Progressive formation of PHF-1 immunoreactivity (**A–C**, brown color) and Gallyas silver-positive inclusions (**D–F**, black color) were age-dependent in CA1 in tau Tg mice showing phospho-tau and NFT-like formation starting from 6 months in the CA1 region. Representative sections of three to five animals used at the age indicated are shown. Scale bar = 25 μm.

tected on the 64-kd band from 3 months and on the 69-kd band from 6 months. Interestingly, murine tau phosphorylated at site Ser396 was also detected in the WT at 10 to 14 months. Tau hyperphosphorylation of Ser202/Thr205 (AT8) was only visible on the 69-kd band from 6 months and of Thr231 (AT180) on both the 64-kd band and the 69-kd band from 6 and 10 months, respectively. Abnormal tau phosphorylation at Thr212/Ser214 (AT100) and Ser422 (AP422/988) occurred from 6 to 10 months, but was only observed on the upper tau band 69-kd tau.

Both mutations used in the present construct were shown to decrease tau binding to microtubules. Thus, we also investigated phosphorylation within the microtubule-binding domains using the 12E8 antibody that recognizes Ser262 and 356. Tau phosphorylation was clearly detected as soon as 3 months. As previously described, the antibody also labeled the AD tau triplet but not a sample of a brain with Pick's disease (PiD).[22] Altogether, these data indicated that there is no PiD-like phosphorylation pattern in THY-Tau22 mice.

Neurofibrillary Inclusions in THY-Tau22 Mice

Neurons containing aggregated tau were identified by traditional Gallyas silver staining in the pyramidal cell layer of the CA1 region (Figure 3) and the frontal cortex at 6 months. The number of neurons stained significantly increased with age. In addition, by 12 months argyrophilic staining is also detected in the DG, the CA3 region, and the amygdala (data not shown). Moreover, ghost tangles were detected in CA1 at 12 months (Figure 6, F–G) by combining Gallyas silver staining with AT8 and hematoxylin as a nuclear counterstain.

Ultrathin sections of the Ammon's horn layer of the hippocampus of tau Tg mice were examined by transmitted electron microscopy to study the ultrastructural aspects of the neuronal inclusions. Pyramidal neurons containing large cytoplasmic fibrillary inclusions are regularly detected in THY-Tau22 mice (Figure 5, A and C). Most of these inclusions were composed of bundles of regularly spaced straight filaments (Figure 5B). These filaments had a mean diameter of 19.4 ± 1.5 nm (mean ± SD). Occasionally, we also observed wider filaments (mean largest diameter of 31.9 ± 2.5 nm; Figure 5D) showing regular constrictions every 129.3 ± 17.4 nm.

Cell Loss and Neurodegeneration in THY-Tau22 Mice

Neurodegeneration is one of the hallmarks of AD brain and is mainly observed in the brain areas affected by tangles and plaques, such as the Ammon's horn, hippocampus, and parietal cortex. In THY-Tau22 mice staining with the nuclear dye DAPI decreased from 12 months onwards in the CA1 region, indicating a progressive cell loss in THY-Tau22 mice (Figure 6, A–D). A decrease in cell number and in staining intensities was observed. At 17 months there was a clear decrease in cell size as well (Figure 6D).

To confirm the cell loss observed with DAPI staining, sections from the CA1 region of 6- to 15-month-old THY-Tau22 and WT mice were stained with Nissl/cresyl-violet.

A decrease in the density of the pyramidal CA1 cell layer and a 34% decrease in the number of pyramidal neurons were evident in THY-Tau22 mice by 12 months (Figure 6E; $^{**}P < 0.01$). At 12 months holes in the CA1-cell layer were also detected, seeming to be attributable to dying cells not being replaced, and at 15 months the size of the pyramidal neurons were also reduced (data not shown).

Gliosis in THY-Tau22 Mice

Reactive astrocytes and microglia cause neuronal damage and therefore play critical roles in the development and progression of AD. Although, gliosis is tightly associated to senile plaques, the near environment of neuronal tangles is affected as well. An increase in the number of astroglial GFAP-positive cells is observed in the hippocampal hilus of aged THY-Tau22 mice (Figure 7), as well as in the cerebral cortex, corpus callosum, CA1 region, and the CA3 region (data not shown). The number of GFAP-positive cells increases with age in both WT and Tg mice. The overall number of microglial cells, visualized by binding to lectin, is also slightly increased in THY-Tau22 mice. Interestingly, there is an accumulation of astroglial and microglial cells near the vicinity of neurons containing large amounts of phospho-tau (Supplementary Figure S1 at *http://ajp.amjpathol.org*).

Decreased Synaptic Transmission in THY-Tau22 Mice

To determine whether the tau pathology in THY-Tau22 mice results in alterations in synaptic transmission, we examined the ability to generate excitatory synaptic responses in the hippocampus of tau Tg mice. Field excitatory postsynaptic potentials (EPSPs) were elicited in the CA1 area by stimulating the Schaffer collaterals with increasing intensities (input/output plots). In 6- to 7-month-old THY-Tau22, there was no alteration in the size of the synaptic responses compared to WT controls (Figure 8A). By contrast, a marked decrease in synaptic excitability was observed in 14- to 15-month-old animals (Figure 8B). The mean amplitude of the EPSPs at the highest stimulation intensity (300 μA) was 0.289 $\pm$ 0.045 mV and 1.24 $\pm$ 0.050 mV for THY-Tau22 mice and WT controls, respectively. These data suggest a loss or malfunction of the synapses in THY-Tau22 mice by 80%. To evaluate further the properties of these synapses, we examined their capacity to express LTP, a form of synaptic plasticity that is believed to be involved in memory formation,[25] in response to a tetanic stimulation. In 6- to 7-month-old animals, the mean LTP was 193 $\pm$ 21% and 206 $\pm$ 16% in WT and THY-Tau22 mice, respectively. These values were not significantly different ($P > 0.6$; unpaired *t*-test). Similarly, in 14- to 15-month-old animals, the amount of LTP was 185 $\pm$ 32% and 186 $\pm$ 21% in WT and THY-Tau22

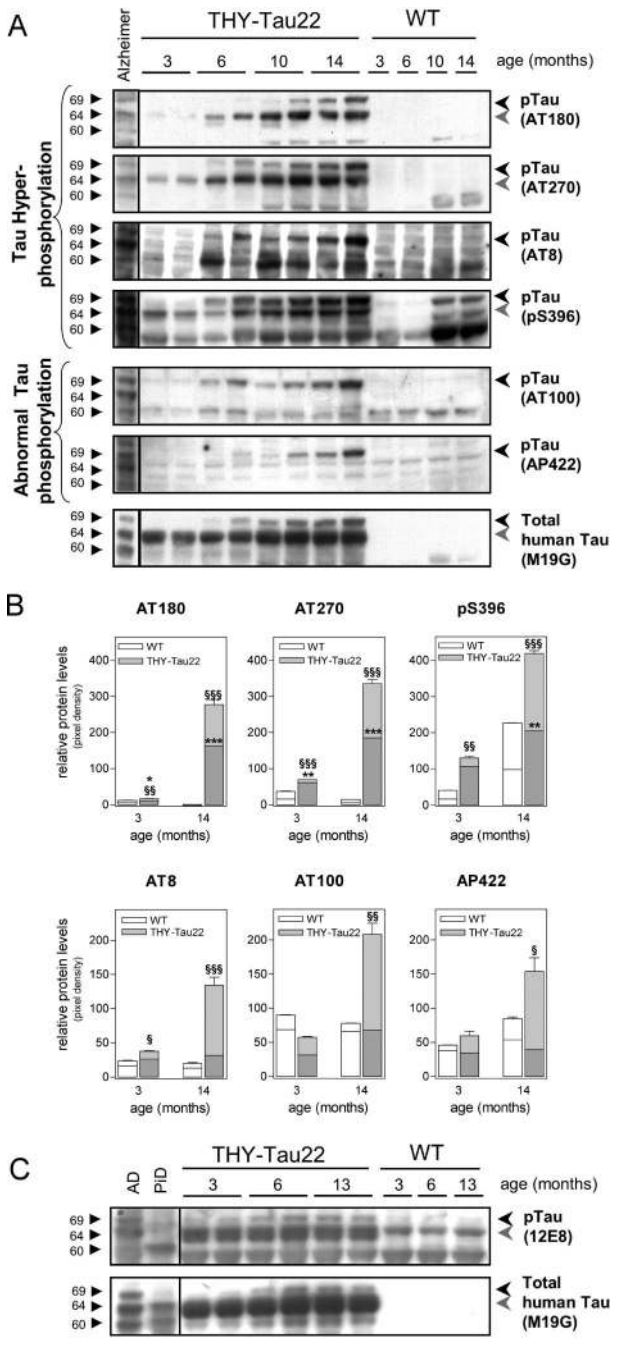

Figure 4. Increase of tau hyperphosphorylation and abnormal tau phosphorylation in the aged THY-Tau22 mouse brain. **A:** Immunoblot analysis of the major AD-relevant tau phosphorylation epitopes. Hyperphosphorylation of tau in cortex at sites Thr231 (AT180), Thr181 (AT270), Ser202/Thr205 (AT8), and Ser396 are detectable from 3 to 6 months and increase with age. Only phosphorylation of murine tau-Ser396 can be detected in aged WT. Abnormal tau phosphorylation at sites Thr212/Ser214 (AT100) and Ser422 (AP422/988) starts at 6 to 10 months. The levels of total human tau protein increase slightly with age in THY-Tau22 mice. Brain homogenate from an AD patient is loaded in the first lane. Triplets of hyperphosphorylated tau isoforms are indicated (69, 64, and 60 kd). Most antibodies detect a duplet of hyperphosphorylated tau in mice, indicated by the black and gray arrowheads. **B:** Quantification of site-specific tau phosphorylation of three individual blots with at least five animals per age and genotype. Densities of the 64 (bottom bars in dark gray; * = significance) and 69-kd band (top bars in light gray, § = significance) were determined in duplicates. Background noise was subtracted for each lane (unpaired Student's *t*-test, $^{*/\S}P < 0.05$, $^{**/\S\S}P < 0.01$ and $^{***/\S\S\S}P < 0.001$). **C:** Immunoblot of 12E8, an antibody that detects phosphorylation of Ser262 and Ser356, which are microtubule-binding domains 1 and 3. 12E8 allows for the discrimination between AD and PiD. Old tau Tg revealed a phosphorylation profile that is comparable to that found in AD. Note that even endogenous murine tau is detected in the WT and Tg. Representative immunoblots are shown.

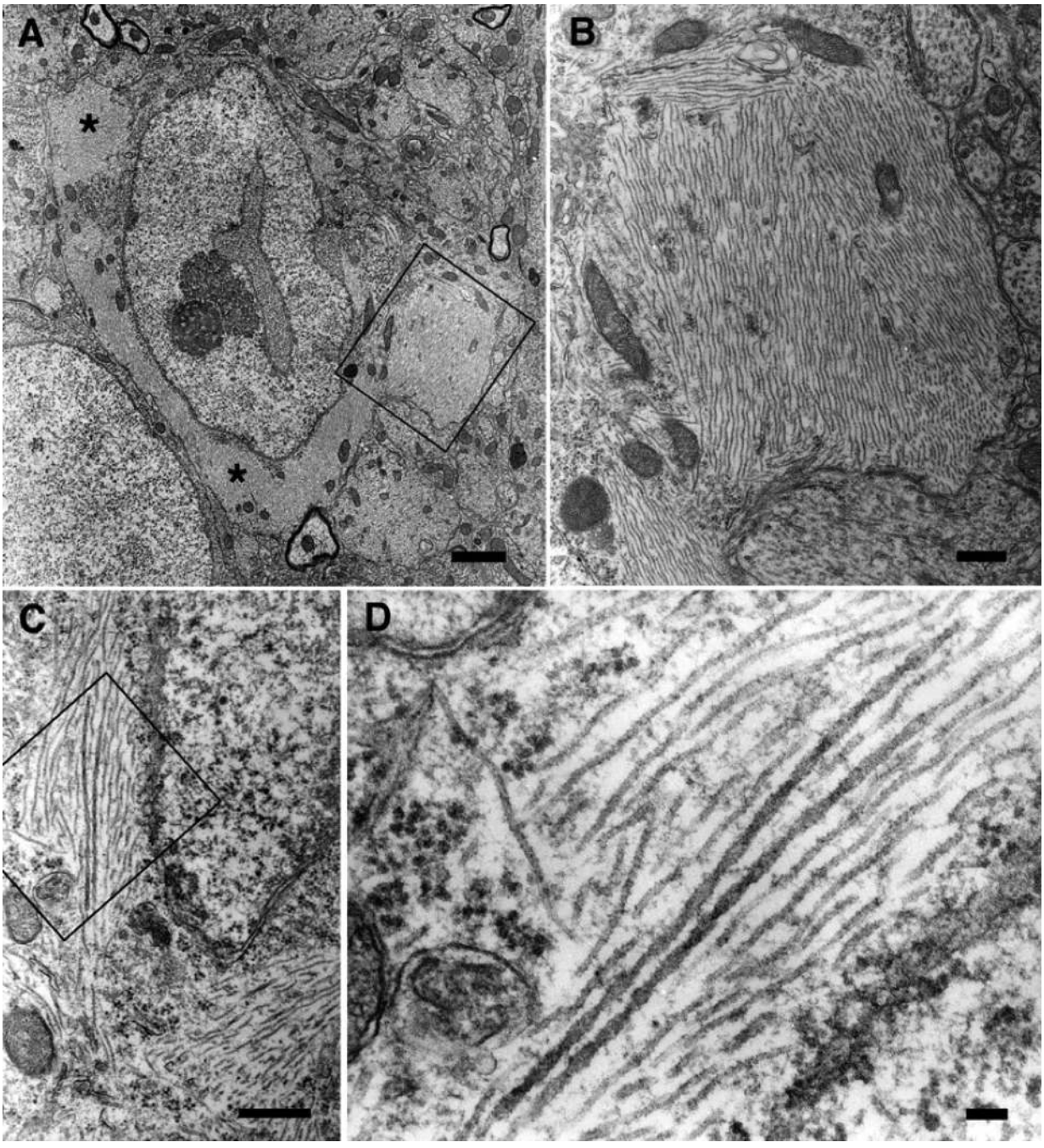

Figure 5. Ultrastructural aspect of fibrillar inclusions in hippocampal neurons from THY-Tau22. **A:** A hippocampal neuron of a 15-month-old THY-Tau22 mouse contains several massive fibrillar inclusions (**asterisks**). **B:** Higher magnification of the **boxed area** in **A**. Fibrillar inclusions are composed of bundles of straight filaments. **C:** Bundles of abnormal filaments in another hippocampal neuron. **D:** Higher magnification of the **boxed area** in **C**, showing the co-existence of straight filaments and occasional wider filaments with regular constrictions. Representative sections are shown. Scale bars: 2 μm (**A**); 0.5 μm (**B**, **C**); 100 nm (**D**).

mice, respectively ($P > 0.9$), indicating that LTP remains normal despite the marked alteration observed at the level of synaptic transmission and suggesting that other synapses remained functional. To verify whether this is a malfunction or a loss of synapses we compared levels of synaptic vesicle-associated proteins, synaptophysin (SYP; major synaptic vesicle protein p38), and synaptotagmin I. Immunoblots of synaptophysin and synaptotagmin displayed no major changes between THY-Tau22 and age-matched WT but a small decrease at 15 months by 20% (Figure 8C). Hence, it seems that the decrease in basal transmission is not only the reason of a synaptic loss but also a malfunction of synapses in aged THY-Tau22.

No Motor Dysfunction in Young and Aged THY-Tau22 Mice

Any tau pathology in spinal cord neurons could lead to motor deficits and paralysis of the limbs and all previous

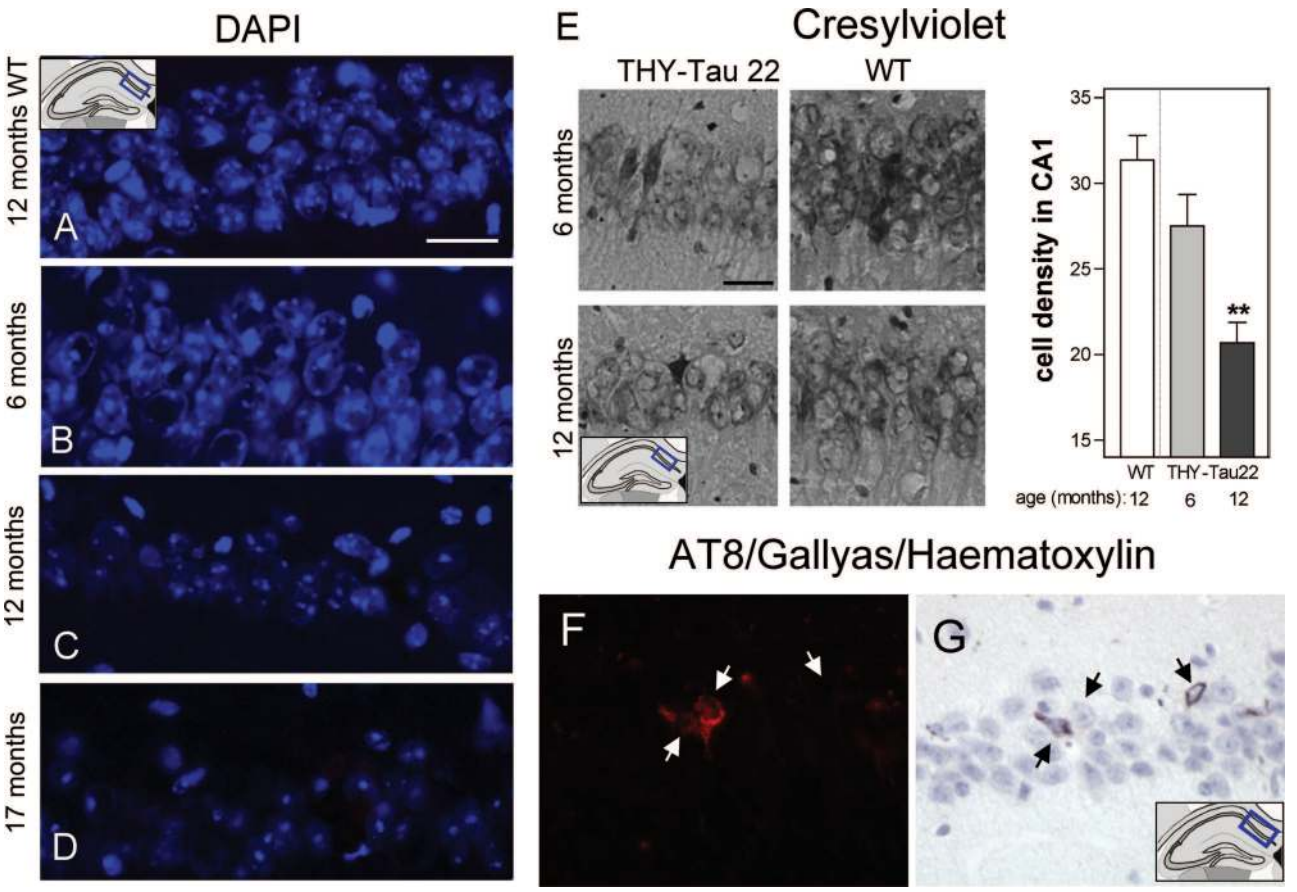

Figure 6. Loss in cell density, neurodegeneration, and ghost tangles in aged THY-Tau22. **A–D:** DAPI-stained neurons of the CA1 cell layer in a 12-month-old WT (**A**) and in THY-Tau22 at 6 (**B**), 12 (**C**), and 17 (**D**) months. Note the decrease in DAPI staining intensity and the reduced cell density with increasing age in the tau Tg mice. Scale bar = 20 μm. **E:** Decrease of cell density in aged THY-Tau22 and semiquantification of Nissl/Cresylviolet-stained cells in the CA1 cell layer (analysis of variance with Bonferroni's post test $^{**}P < 0.01$ Tg versus WT at 12 months; $n = 3$ per age and genotype). Scale bar = 20 μm. **F:** AT8 immunolabeling combined with **G:** Gallyas staining and hematoxylin staining. Three cells with different staining patterns are shown by the **arrows** (from **left** to **right**): **left**: an AT8 and Gallyas-positive cell, with a nucleus; **middle**: an AT8-positive but Gallyas-negative cell, with a nucleus; **right**: a Gallyas-positive and AT8-negative cell, without nucleus. Note the loss of AT8 immunoreactivity and the argyrophilic extracellular NFT in the latter, which corresponds to a late ghost tangle.

Tg mouse models expressing human tau have described the development of motor impairment and spinal pathology in adult and elderly animals.[7,26–28] To demonstrate further that our model does not show a severe spinal cord pathology that could result in motor dysfunction and thereby impair behavior tests that afford proper motor function, spinal cords were dissected for histological and immunohistochemical analyses. Minor traces of human tau became detectable in the spinal cord by 3 to 6 months, and their amount increased slightly in aged mice (Figure 1, B and C, and Figure 2L). No atrophy or morphological changes were observed in sections from spinal cord. Although the detectable amounts of human tau in the spinal cord are relatively low, we assessed their physiological effect.

In a modified Irwin protocol to evaluate general behavior, motion and movability, muscle strength, and some physiological parameters, there was no difference between THY-Tau22 and WT mice, except for the already mentioned decrease in bodyweight and an overall increase in nervous behavior in the THY-Tau22 mice. Male tau Tg mice at all ages (3 to 14 months old, $n = 8$ per group) showed the same ability than the WT animals to balance their way across an elevated wire, to grasp at during 5 seconds, and to climb back on the wire. During the grasping period no limb preferences were observed.

The general motor activity of the Tg animals was analyzed in the elevated plus maze. No changes between THY-Tau22 and WT regarding the numbers of total arm entries, the total distance moved, their running speed, and the time being inactive were observed (Table 2). The only difference found was that the Tgs spent more time in open arms whereas the WTs preferred to explore the enclosed ones and thereby a different number of entries in open arms (Figure 9, A–F). In addition, the tau Tg mice were investigated for their ability to run on a rotating drum (the rotarod). As shown in Table 2, no significant differences were observed. However, there was a small tendency that THY-Tau22 mice could run longer on the rotarod, indicating apparently improved motor skills with a preference in male animals (data not shown). We could demonstrate in subsequent experiments that the size of male WT mice at 6 months (~35 g) was at the limit for an accurate run on the rotarod. Because the THY-Tau22 mice have a reduced size, they apparently show better motor skills compared to their bigger WT littermates. Because of the smaller size of females, this effect was less pronounced in the female sex. However, no dysfunc-

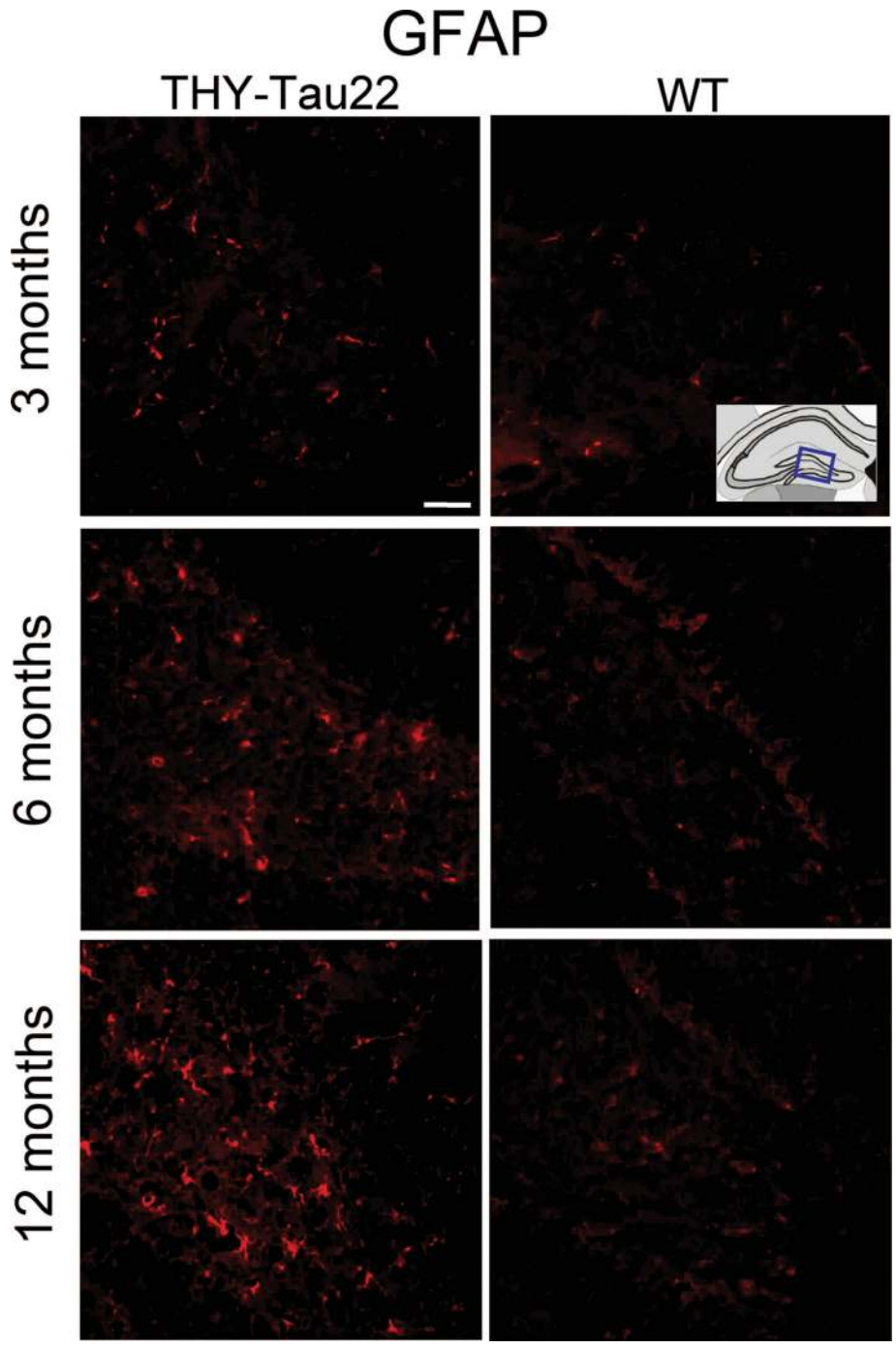

Figure 7. Gliosis in THY-Tau22 mice. GFAP-immunoreactivity in the hippocampal hilus is increased in THY-Tau22 mice compared to WT animals at 3, 6, and 12 months. Representative sections of 10 mice are shown. Scale bar = 20 μm.

tion of motor skills and no signs of motor impairment and paralysis were found in THY-Tau22 up to an age of 18 months.

Behavioral Abnormalities in THY-Tau22 Mice

The most common early symptoms of AD are memory deficits and cognitive impairment. Because no change was observed in motor activity and locomotion, THY-Tau22 mice were assessed in a battery of different behavioral tests to detect any changes in anxiety, cognition, and memory to evaluate the behavioral effects of tau pathology. To examine anxiety, 6-month-old mice were observed in an elevated plus maze (Figure 9A). The time the tau Tg animals spent in the open arms of the plus maze was significantly increased compared to sex-matched littermates (Figure 9, B–F). Non-Tg littermates appeared to recognize their location and preferred to remain within the closed arm of the maze, whereas THY-Tau22 mice tended not to discriminate between the

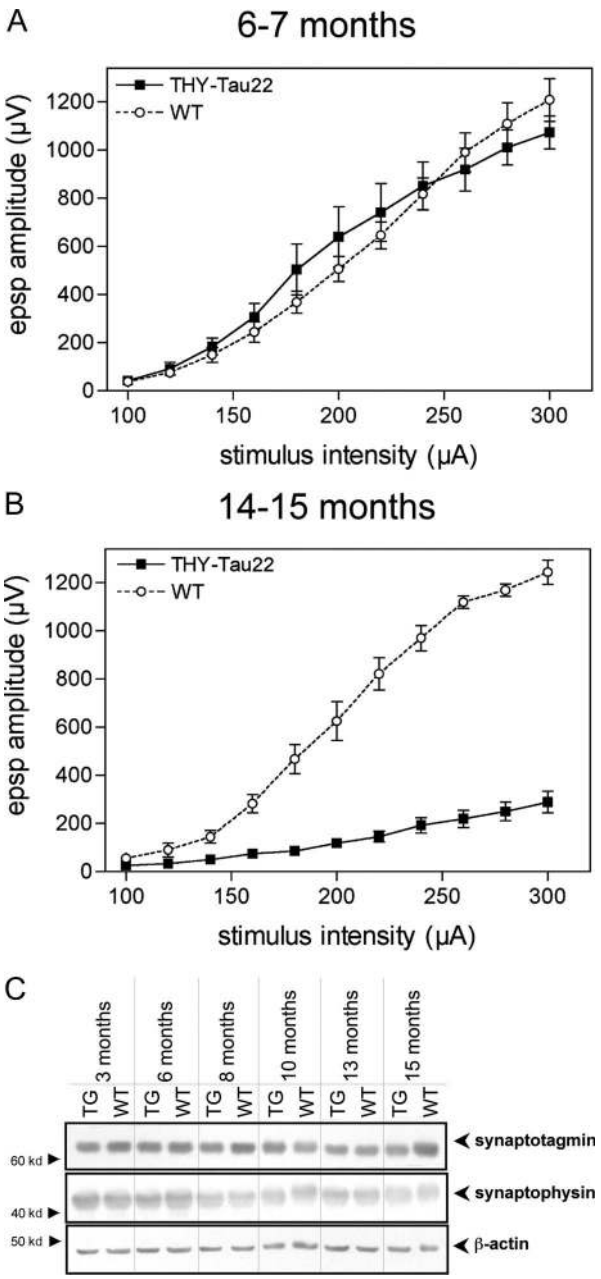

Figure 8. Decreased synaptic transmission in the hippocampus of THY-Tau22 mice. **A:** Input/output plots of the amplitude of the field excitatory postsynaptic potentials in the CA1 area elicited by stimuli of increasing intensity in hippocampal slices prepared from 6- to 7-month-old WT (open circles) and THY-Tau22 Tg mice (filled squares). Two-way analysis of variance of the EPSP amplitude values throughout the 100- to 300-μA stimulation intensity range indicated no significant effect of genotype ($F[1,8] = 0.0931$; $P > 0.7$). **B:** Input/output plots from 14- to 15-month-old animals, indicating impaired synaptic function by 80% compared to age-matched WT. Analysis of variance indicated a highly significant effect of genotype ($F[1,4] = 207.2$; $^{***}P < 0.001$). At least five animals were used per group. **C:** Protein levels of synaptotagmin I and synaptophysin, proteins that are involved in synaptic integrity, are not significantly changed between Tg (THY-Tau22) and WT. Thus, a small decrease by 20% was detected in 15-month-old THY-Tau22. However, a synaptic malfunction of basal transmission in old THY-Tau22 appears not to be due only to a minor loss of synaptic proteins. Representative immunoblots are shown.

closed and open arms of the maze. As indicated above, these findings cannot be explained by differences in locomotor activity because the overall spontaneous locomotion and general motor activity were not altered between the genotypes (Table 2).

Table 2. No Changes in Overall Motor Activity and No Motor Deficits in THY-Tau22 Mice

	Sex	*n*	Mean (cm) ± SEM
Motor activity			
Total distance in cm			
THY-Tau22	M	8	806.4 ± 84.63
WT	M	8	867.5 ± 90.42
THY-Tau22	F	7	896.2 ± 119.1
WT	F	8	786.2 ± 38.70
Inactive time in seconds			
THY-Tau22	M	8	213.0 ± 6.80
WT	M	8	202.4 ± 6.75
THY-Tau22	F	7	212.4 ± 6.62
WT	F	8	214.0 ± 5.79
Total number of arm entries			
THY-Tau22	M	8	23.63 ± 3.04
WT	M	8	26.25 ± 2.26
THY-Tau22	F	7	19.86 ± 3.39
WT	F	8	24.13 ± 1.76
Motor skills on the rotarod			
Time running at 25 rpm in seconds			
THY-Tau22	F	7	46.75 ± 16.47
WT	F	8	35.00 ± 13.60

Data of total distance walked, inactive time, and number of total arm entries in the elevated plus maze (EPM) was analyzed for general motor activity. No changes between tau transgenics and age-matched WTs from the same litter could be determined. To reveal whether the minor expression of transgene in spinal cord has an effect on motor function in THY-Tau22, the motor skills of tau transgenics and WTs were determined on the rotarod. No differences could be found indicating a normal motor function in THY-Tau22. All data were not statistically significant between transgenics and WTs (unpaired Student's *t*-test, $P > 0.05$).

THY-Tau22 mice (at 2 to 3, 7, 10 and 14 months; $n = 8$ per group) were also subjected to a cognitive test for spatial learning and memory, the MWM. During a 4-day training period, the mice were tested in four trials per day for their ability to locate a hidden platform aided by visual clues surrounding the water pool. The WTs quickly learned to find the platform, whereas the learning of the tau Tgs was delayed (for 10-month mice see Figure 10A). The delayed learning in the tau mice was significant on day 2 and day 3 (Figure 10, A and D–E), but by day 4 of testing there was no difference between THY-Tau22 and WT mice (Figure 10A). Figure 10B shows that there was also a significant impairment in learning on training day 3 in THY-Tau22 mice at 2 to 3 months, 10 months, and 14 months.

To examine spatial memory performance mice that had previously received a 4-day training period did not receive training for 5 days and were then tested on day 9 for their ability to search for the platform in the same water pool with visual clues, but where the platform had been removed. At 10 and 14 months the THY-Tau22 mice were significantly poorer at remembering the quadrant where the platform had been placed than age-matched WT (Figure 10C). The time the THY-Tau22 mice spent in the goal quadrant was below the chance level of 15 seconds, ie, the time expected for mice who had never received training (compare also Figure 10, F and G). In addition, in a pilot study with a slightly modified protocol, 6-month-old

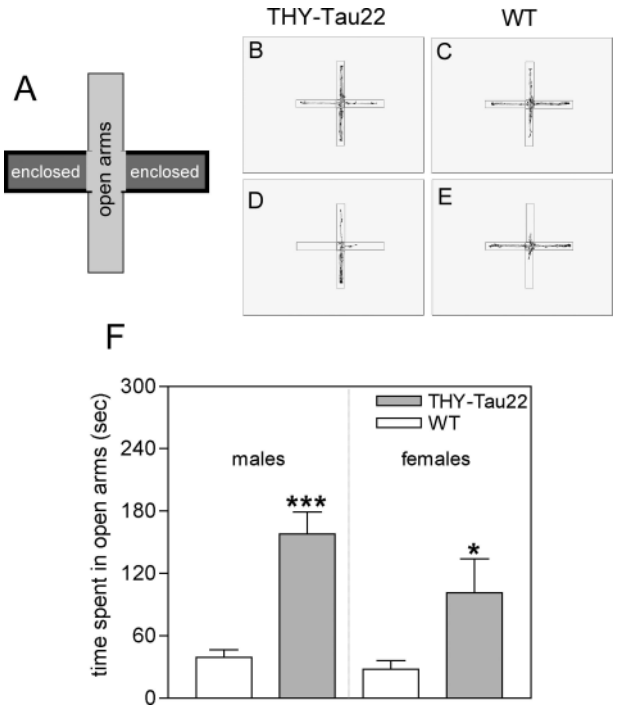

Figure 9. Altered anxiety in the elevated plus maze in THY-Tau22 mice. Impaired anxiety in THY-Tau22 mice. **A:** Model of the elevated plus maze (EPM) used with two enclosed arms and two open arms. The mice were placed in the middle facing an open arm and their movements were recorded throughout 5 minutes. Representative locomotion traces for THY-Tau22 (**B**, **D**) and WT (**C**, **E**) mice in the elevated plus maze. **F:** THY-Tau22 mice spend more time in the open arms of the elevated plus maze compared to their littermate WTs (157.9 ± 21.23 seconds for male THY-Tau22 versus 39.29 ± 7.334 seconds for male WT, $^{***}P < 0.0001$; 101.3 ± 32.62 seconds for female THY-Tau22 versus 27.95 ± 8.078 seconds for female WT, $^{*}P < 0.05$; $n = 8$ per group, 6 months old).

THY-Tau22 mice also had significantly delayed escape latencies and spent less time in the goal quadrant in the probe test (data not shown).

Discussion

We have generated and characterized a new tau Tg mouse model expressing human 4-repeat tau with the double mutations G272V and P301S under the Thy1.2 promoter in the absence of any motor dysfunction. These mice were generated using the htau46 isoform (2+ 3− 10+), as it is one of the most common tau isoforms in human brain[29] and adult rodents.[30] G272V is one of the first described mutation in FTDP-17 in the first microtubule binding repeat motif in all tau isoforms[31,32] whereas P301S is found in the second microtubule binding repeat motif in 4R tau isoforms. In addition, the P301S mutation shows a very early mean age of onset for FTD in man.[33]

Compared with other tau Tg mouse models, the THY-Tau22 model has a rather early onset of tau pathology starting at 3 to 6 months (Table 3), especially for a heterozygous genotype. The variability among the individuals was very small. Although in a recent published inducible tau model with expression of P301L-tau, NFT-like formations occur at 3 months,[9] in most other hemizygous tau Tg mice tau pathology starts at 5 to 15 months.[7,8,10,12–16,26,34,35] Moreover, most of them suffer from motor dysfunction after 10 months.[7,10,14,16,26,34,36] Interestingly, in a Tg mouse model with tau cDNA bearing three FTDP-17 mutations[37] the tau pathology started particularly early at 1.5 to 3 months. This suggests that the number of mutations may accelerate the onset of tau pathology. Because we wanted to study the early stages of tau accumulation rather than the very late we choose to use two mutations to have a greater time window with a good resolution for each stage of the pathology in a heterozygous background.

To achieve a strong transgene expression in neurons the Thy1.2 promoter was chosen.[21] Other promoters are either not neuron-specific such as the platelet-derived growth factor (PDGF) promoter or weak such as the CaMK-II (Ca^{2+}-calmodulin-dependent kinase II) promoter. The main criticism of the Thy1.2 promoter is its strong efficiency in motor neurons. Thus, in the selection of mice lines for further characterization we excluded lines with high transgene expression in the spinal cord to avoid potential motor deficits that could prevent characterization of the mice throughout their whole lifespan and in behavior tests. Altogether, these criteria allowed for the selection of the THY-Tau22 mouse line. In this model, tau is predominantly expressed in the brain, and the mice do not display any motor deficits. These tau mice also display some of the phenotypic changes that have been previously observed in AD tau pathology. These include hyperphosphorylation and abnormal phosphorylation of tau, the presence of NFT-like formations, loss of functional synapses, and astrogliosis. These biochemical and pathophysiological changes are also accompanied by mild cognitive impairment.

The use of FTDP-17 mutations raises the problem of THY-Tau22 mouse as a model of tauopathy rather than AD. It is clear that the present model does not display amyloid pathology and thus, it is not a full AD model. However, our goal was to develop a model close to the tau pathology in AD. There are numerous features indicating that the pathology observed in this model is closer to that found in AD than in other tauopathies. For instance, FTD is a pool of dementia, which includes not only FTDP-17 (with tau mutations) but also dementia lacking distinctive histopathology (DLDH), PiD, and other entities. Regarding DLDH, the model shows tau aggregation and thus, by definition does not belong to DLDH. FTDP-17 is heterogeneous at both neuropathological and biochemical levels. For instance, in patients presenting the G272V mutation, the neuropathological hallmarks are Pick bodies.[31,32] Similarly, patients with P301S mutation exhibit heterogeneous clinical and pathological features (parkinsonism, corticobasal degeneration, or fronto-temporal dementia) and both NFT and glial fibrillary tangles.[38–41] The present model, even with two mutations on the tau cDNA, does not display such heterogeneity and may not be clearly identified as a model of FTDP-17. This model is not typical of Pick disease (PiD) because tau pathology is not made of three-repeat tau isoforms and tau filaments do not form Pick bodies. In addition, tau phosphorylation at Ser262 can be used to discriminate between PiD and AD or corticobasal degeneration.[22] Tau

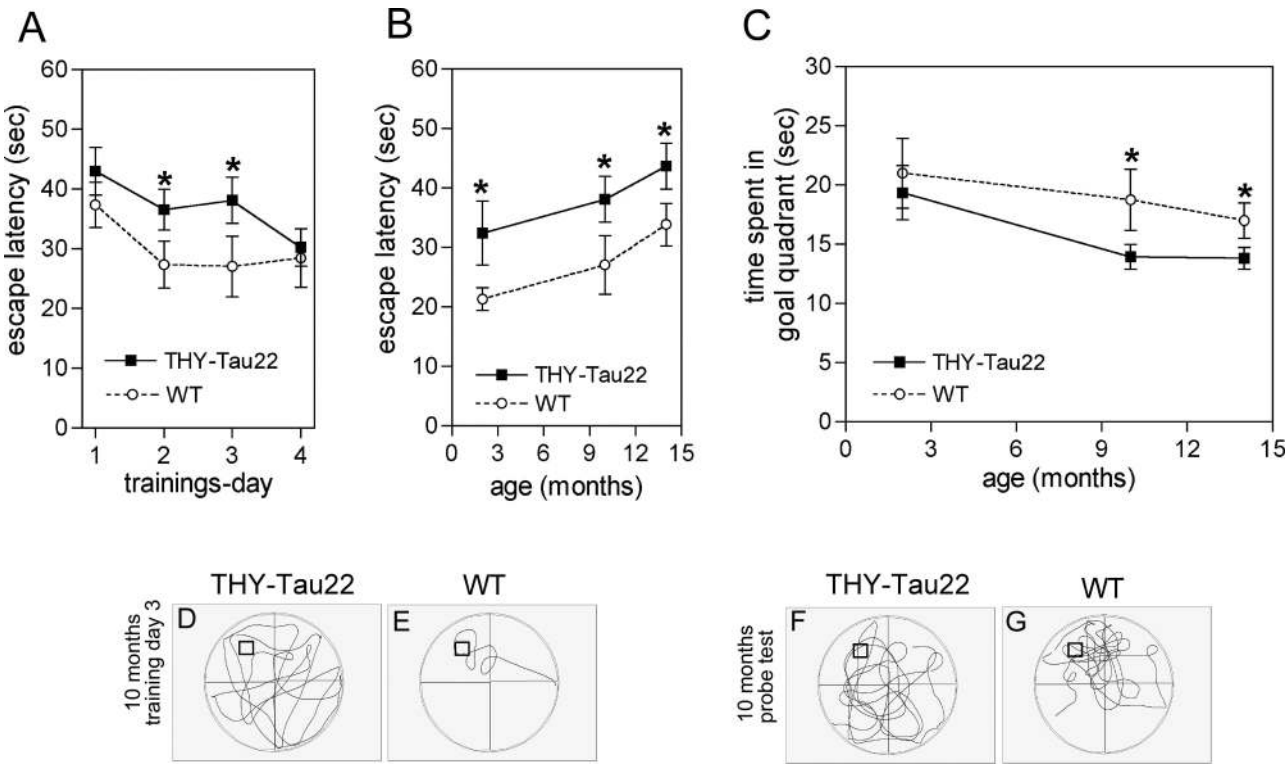

Figure 10. Retarded learning and reduced memory in THY-Tau22 mice. Delayed learning in the MWM in THY-Tau22 mice. **A:** Escape latency, the time to find the hidden platform in the MWM, during the 4-day training period in 10-month-old THY-Tau22 mice (filled squares, $n = 8$) and WT (open circles, $n = 8$). Day 1, THY-Tau22 42.95 ± 3.979 seconds versus WT 37.33 ± 3.815 seconds; day 2, THY-Tau22 36.52 ± 3.412 seconds versus WT 27.34 ± 3.894 seconds, $^{*}P < 0.05$; day 3: THY-Tau22 38.08 ± 3.849 seconds versus WT 27.00 ± 4.912 seconds, $^{*}P < 0.05$; day 4, THY-Tau22 30.21 ± 3.140 seconds versus WT 26.51 ± 4.901 seconds; Two-way analysis of variance, $^{*}P > 0.05$ for genotype, $^{*}P > 0.05$ for learning). **B:** Escape latency in MWM in 2- to 3-, 10- and 14-month-old THY-Tau22 and WT on training day 3. THY-Tau22 display a delay in learning (two-way analysis of variance $^{**}P < 0.01$ for genotype, $^{*}P < 0.05$ for age, $n = 8$ per group). **C:** Five days after the last training the platform was removed and a probe test was performed. The time the mice spent in the quadrant where the platform used to be (= goal quadrant) is plotted against age. Aged animals show a mild memory deficit compared to age-matched WTs ($n = 8$ per group). Representative locomotion traces of THY-Tau22 (**D**, **F**) and WTs (**E**, **G**) during the learning period (**D**, **E**) and the probe test (**F**, **G**).

phosphorylation at Ser262 is clearly detected in THY-Tau22. Thus, the present model is not representative of FTDP-17, DLDH, and PiD. Nevertheless, progressive supranuclear palsy and corticobasal degeneration exhibit aggregation of 4R tau isoforms such as in the present model. However, once again, there is no motor deficit in the present model whereas motor deficits are observed in these pathologies. Taken together, this is the first tau mouse model demonstrating AD-like tau pathology without displaying any motor deficits.

Tau phosphorylation was observed at the major sites involved in both abnormal phosphorylation and hyperphosphorylation of tau in AD.[42] However, hyperphosphorylation and abnormal phosphorylation have also been described in many stress conditions including hibernation and starvation.[43,44] These phenomena were described as reversible, but it seems not the case in tau Tg mice.[9,28] In the present model, tau hyperphosphorylation and abnormal phosphorylation increase with age. It is correlated with the appearance of NFT, silver staining, and filaments. Thus, hyperphosphorylation and abnormal phosphorylation are clearly pathological in the present work. Moreover, the age-related increase in phospho-tau immunoreactivity is comparable to that found in AD brains at different Braak stages.[45] The abnormal tau phosphorylation at Thr212/Ser214 increases with age and is well correlated with the number of NFT-like formations, indicating that a dysregulation in tau phosphorylation may be instrumental in tau aggregation, as suggested previously in P301L mice.[46] The observed 64-kd tau band corresponds to a hyperphosphorylated tau variant, whereas the 69-kd tau band is the abnormally phosphorylated form of tau that has been described in human AD brains.[29] Therefore, it seems that the presence of the 69-kd tau band is necessary for the evolution of NFTs.

Phospho-tau immunoreactivity in neurites and fiber tracts of the whole hippocampus started early, increased up to 6 months (Figure 3B) and then decreased with a degeneration of the axonal tracts (Figure 3C). The size of AT8 immunoreactive cell bodies decreased in the frontal cortex, the CA1 and CA3 region in old THY-Tau22, suggesting that neurons containing tau phosphorylated at sites Ser202/Thr205 (AT8) are more prone to undergo degeneration. Similar findings indicating that tau phosphorylation at sites Ser202/Thr205 correlates with the severity of neuronal cytopathology have been observed in AD brain.[47] By contrast, recent observations suggest that extensive cell death can occur independently of formation of NFT-like formations[35] and that NFTs do not invariably cause neuron death[9] implying an NFT-independent mechanism of neuronal death.

Table 3. Comparison of the Most Common Tau Transgenic Models and Other Models with Tauopathy

Tau transgenic models					
Promoter	Mutation	Begin of tau brain pathology	Phopho-tau in spinal cord	Motor impairment	Reference
PrP	P301L	5 months	Detectable at 5 months	Yes at 6.5 months (hemizygous)	7
CamK-II (inducible *tet-off*)	P301L	2.5 months	n.d. at 2.5 months	Yes at 9.5 months	9, 28
Thy1.2	P301L	3 months	Detectable at 3 months	Yes (muscle atrophy and weakness)	8
Thy1.2	P301S	5 months	Detectable at 5 months	Yes at 5 months (homozygous)	10
Thy1	G272V P301L R406W	1.5 months	Detectable at 1.5 months	No abnormality up to 12 months	37
CamK-II	R406W	5 months	Detectable at 5 months	No abnormality up to 23 months	13
Thy1.2	G272V P301S	3 months	Minor traces at 3 to 6 months	No abnormality up to 18 months	Present study
APP or PS1 and tau double/triple-transgenic models					
Promoter	Transgene expression	Begin of tau brain pathology	Phopho-tau in spinal cord	Motor impairment	Reference
Thy1.2 (Tau, APP), PS1-KI	$Tau_{P301L}xAPP_{sw}xPS1_{M146V}$	12 months	No data available	No data available	63
PrP (Tau), PrP(APP)	$Tau_{P301L}xAPP_{sw}$	6 months	3 months	Yes	60
Other transgenic models with tau pathology					
Promoter	Targeted gene	Begin of tau brain pathology	Motor impairment		Reference
–	*pin1 (−/−)*	2 years	No		64
NSE	*p25*	4 months	No paralysis but increased spontaneous locomotor activity		65

CamK-II, Ca^{2+}-calmodulin-dependent kinase II; KI, knockin; NSE, neuron-specific enolase; n.d., not detectable; Pin1, peptidyl-prolyl cis/trans isomerase 1; PrP, prion protein promotor; (−/−), knockout.

In summary, this model shows a rather high resolution of different steps in tau pathology that allows us to investigate the very early stage when tau phosphorylation starts at the first sites in the CA1 and cortex (3 months), a stage when hyperphosphorylation is much more advanced, more sites are involved in tau phosphorylation, abnormal phosphorylations begins, the pathology spreads to the DG, and more NFT-like inclusions occur (6 months), a stage with massive hyper and abnormal phosphorylation, the occurrence of phospho-tau and NFT-like inclusions at many anatomical sites, and the beginning of degenerative processes (10 months) and finally a stage with neurodegeneration, advanced cell loss, malfunction of hippocampal synapses, and ghost tangles (14 months). In our model tau pathology starts in CA1 and less pronounced in frontal cortex and then spreads to DG, other cortical regions, and amygdala.

GFAP-positive cells are detected rather early in the pathology of THY-Tau22 mice and increase with age but are not a striking feature of the model. In a P301S tau model[48] and a Tg mouse overexpressing the shortest human tau isoform,[16] a similar astrogliosis and increased microgliosis has been shown to concentrate around tau-positive nerve cells, mainly in the brainstem and spinal cord. In a P301L tau model astrogliosis was also found surrounding phospho-tau-positive neurons[8] in the amygdala and cortex. However, the astrogliosis observed in all of these tau Tg models is relatively mild compared to that found in APP- and APP/PS1-Tg mice[49] and in AD brain.[5]

The tau pathology of THY-Tau22 mice is also accompanied by a deficit in synaptic transmission in the hippocampus. The reduction in basal synaptic transmission indicates that there is a malfunction of the synapses in the hippocampus. Because no significant changes in proteins involved in synaptic vesicles were found and because the response to LTP remained normal, despite the marked alterations observed at the level of synaptic transmission, this suggests that the remaining synapses were functional. Decreases in hippocampal neural activity have also been detected in old V337M tau Tg mice.[12] In AD synaptic loss is closely related to APP and amyloid plaques.[50] AD-relevant mutations of APP were shown to contribute to synaptic dysfunction in Tg animals[51] and to appear, by contrast to our model, rather early in pathology.

The neurodegeneration in THY-Tau22 is rather mild compared to that observed in AD. Additional stereological analysis will be necessary to document further the neuronal loss in the entorhinal cortex and other cortical regions. Neurodegeneration and cell loss have also been observed in other tau Tg mouse models with tau mutations at sites P301S,[10] P301L,[7,8] V337M,[12] and R406W.[14,36,37]

Before subjecting the tau Tg mice to a behavioral test for learning and memory, we evaluated whether minor expression of transgene in spinal cord in old animals caused any motor dysfunction. Young and aged THY-Tau22 did not show any changes in motion, coordination, muscle strength, motor skills, and general motor behavior compared to the WTs. This indicates that the traces of phospho-tau found in the spinal cord of elderly Tgs are not sufficient to cause motor deficits. The absence of motor dysfunction is essential for a proper analysis of rodents in behavioral studies. Behavioral tests are dependent on the animal's movement (running, swimming) and motor coordination. Any motor impairment caused by transgene expression severely impairs behavior testing, is extremely unfavorable for the test outcome, and makes it impossible to interpret the data. All other previous common tau Tg mouse models display sooner or later pathological denervation, atrophy, or phosphorylated tau in the spinal cord[7,8,10,14,27,28] accompanied by motor impairment or even paralysis. Although all these tau models provide a beautiful histopathology similar to AD and contributed a lot to understand the role of tau in AD, the occurrence of even minor motor deficits makes it hard to analyze properly their behavior data.

The general motor behavior of THY-Tau22 was not changed. This is an important advantage of the THY-Tau22 model because decreased locomotion[13] or increased spontaneous locomotion and increased exploratory behavior[12,52] has been observed in other tau models. The reduced anxiety-like behavior observed in the elevated plus maze could be attributable to the transgene expression and/or the expression of phospho-tau in amygdala nuclei, because amygdala lesions have been associated with anxiolytic effects in this maze test.[53] A similar decrease in anxiety has also been observed in V337M tau Tgs,[12] although this was also accompanied by an increase in spontaneous locomotion.

In the MWM, a hippocampal-dependent visuo-spatial learning task, the early presence of phospho-tau in the hippocampus could explain the delayed learning in THY-Tau22 mice at all ages. However, because transgene expression under the Thy1.2 starts at postnatal day 6,[21] we cannot exclude that postnatal development involving neuronal sprouting, number of neuronal connections, and neuronal targeting is affected by the transgene, as well. The fact that spatial memory performance is only impaired at 10 and 14 months could be explained, at least in part, by the increase in the number of argyrophilic inclusions, because the number of NFTs is correlated with the severity of cognitive dysfunction in AD.[54] No significant differences in spatial learning and memory were observed in P301L tau mice[55] and V337M tau mice.[12] However, R406W tau mice displayed reduced memory in a passive avoidance test[14] and impairment in a test for associative memory and cued fear conditioning.[13] Arendash and co-workers[55] have also demonstrated a significant correlation between the number of tau-positive neurons in the neocortex of JNPL3 mice and delayed escape latency in the MWM. A recently published mouse model with suppressible tauP301L expression[9] showed motor dysfunction at 10 months that impairs the swim speed in the MWM.[28]

The present tau Tg model exhibits only a part of the full AD pathology. Its generation aims to understand the evolution and mechanisms of pathogenic tau aggregation in AD. In AD, tangle formation occurs early in pathogenesis and is proceeded by the generation of amyloid plaques.[56] It is still a subject of discussion whether APP is involved in tau aggregation or vice versa.[57,58] In our model, A-β immunoreactivity and Congo Red staining were not detectable, and APP metabolism was not altered (data not shown). In the future, it would be of interest to analyze in the present model the effect of amyloid on neurofibrillary degeneration propagation as it was described in the models of Götz and colleagues[59] and Lewis and colleagues.[60]

In conclusion, THY-Tau22 mice display the main features of tau pathology and several of the pathophysiological disturbances observed in AD in the absence of any motor deficits. This mouse model therefore represents a valuable tool to understand further the role and the mechanisms regulating pathological degeneration during tau hyperphosphorylation and tau aggregation in AD.

Acknowledgments

We thank Kunie Ando for helping with biochemical analysis and André Delacourte for providing human brain homogenates.

References

1. Arendt T, Bigl V, Arendt A, Tennstedt A: Loss of neurons in the nucleus basalis of Meynert in Alzheimer's disease, paralysis agitans and Korsakoff's Disease. Acta Neuropathol (Berl) 1983, 61:101–108
2. Scott SA, DeKosky ST, Sparks DL, Knox CA, Scheff SW: Amygdala cell loss and atrophy in Alzheimer's disease. Ann Neurol 1992, 32:555–563
3. West MJ, Coleman PD, Flood DG, Troncoso JC: Differences in the pattern of hippocampal neuronal loss in normal ageing and Alzheimer's disease. Lancet 1994, 344:769–772
4. Gomez-Isla T, Price JL, McKeel Jr DW, Morris JC, Growdon JH, Hyman BT: Profound loss of layer II entorhinal cortex neurons occurs in very mild Alzheimer's disease. J Neurosci 1996, 16:4491–4500
5. Blasko I, Stampfer-Kountchev M, Robatscher P, Veerhuis R, Eikelenboom P, Grubeck-Loebenstein B: How chronic inflammation can affect the brain and support the development of Alzheimer's disease in old age: the role of microglia and astrocytes. Aging Cell 2004, 3:169–176
6. Coleman P, Federoff H, Kurlan R: A focus on the synapse for neuroprotection in Alzheimer disease and other dementias. Neurology 2004, 63:1155–1162
7. Lewis J, McGowan E, Rockwood J, Melrose H, Nacharaju P, Van Slegtenhorst M, Gwinn-Hardy K, Paul Murphy M, Baker M, Yu X, Duff K, Hardy J, Corral A, Lin WL, Yen SH, Dickson DW, Davies P, Hutton M: Neurofibrillary tangles, amyotrophy and progressive motor disturbance in mice expressing mutant (P301L) tau protein. Nat Genet 2000, 25:402–405
8. Gotz J, Chen F, Barmettler R, Nitsch RM: Tau filament formation in transgenic mice expressing P301L tau. J Biol Chem 2001, 276: 529–534
9. Santacruz K, Lewis J, Spires T, Paulson J, Kotilinek L, Ingelsson M, Guimaraes A, DeTure M, Ramsden M, McGowan E, Forster C, Yue M, Orne J, Janus C, Mariash A, Kuskowski M, Hyman B, Hutton M, Ashe

KH: Tau suppression in a neurodegenerative mouse model improves memory function. Science 2005, 309:476–481
10. Allen B, Ingram E, Takao M, Smith MJ, Jakes R, Virdee K, Yoshida H, Holzer M, Craxton M, Emson PC, Atzori C, Migheli A, Crowther RA, Ghetti B, Spillantini MG, Goedert M: Abundant tau filaments and nonapoptotic neurodegeneration in transgenic mice expressing human P301S tau protein. J Neurosci 2002, 22:9340–9351
11. Gotz J, Tolnay M, Barmettler R, Chen F, Probst A, Nitsch RM: Oligodendroglial tau filament formation in transgenic mice expressing G272V tau. Eur J Neurosci 2001, 13:2131–2140
12. Tanemura K, Murayama M, Akagi T, Hashikawa T, Tominaga T, Ichikawa M, Yamaguchi H, Takashima A: Neurodegeneration with tau accumulation in a transgenic mouse expressing V337M human tau. J Neurosci 2002, 22:133–141
13. Tatebayashi Y, Miyasaka T, Chui DH, Akagi T, Mishima K, Iwasaki K, Fujiwara M, Tanemura K, Murayama M, Ishiguro K, Planel E, Sato S, Hashikawa T, Takashima A: Tau filament formation and associative memory deficit in aged mice expressing mutant (R406W) human tau. Proc Natl Acad Sci USA 2002, 99:13896–13901
14. Ikeda M, Shoji M, Kawarai T, Kawarabayashi T, Matsubara E, Murakami T, Sasaki A, Tomidokoro Y, Ikarashi Y, Kuribara H, Ishiguro K, Hasegawa M, Yen SH, Chishti MA, Harigaya Y, Abe K, Okamoto K, St George-Hyslop P, Westaway D: Accumulation of filamentous tau in the cerebral cortex of human tau R406W transgenic mice. Am J Pathol 2005, 166:521–531
15. Brion JP, Tremp G, Octave JN: Transgenic expression of the shortest human tau affects its compartmentalization and its phosphorylation as in the pretangle stage of Alzheimer's disease. Am J Pathol 1999, 154:255–270
16. Ishihara T, Hong M, Zhang B, Nakagawa Y, Lee MK, Trojanowski JQ, Lee VM: Age-dependent emergence and progression of a tauopathy in transgenic mice overexpressing the shortest human tau isoform. Neuron 1999, 24:751–762
17. Duff K, Knight H, Refolo LM, Sanders S, Yu X, Picciano M, Malester B, Hutton M, Adamson J, Goedert M, Burki K, Davies P: Characterization of pathology in transgenic mice over-expressing human genomic and cDNA tau transgenes. Neurobiol Dis 2000, 7:87–98
18. Lo MM, Fieles AW, Norris TE, Dargis PG, Caputo CB, Scott CW, Lee VM, Goedert M: Human tau isoforms confer distinct morphological and functional properties to stably transfected fibroblasts. Brain Res Mol Brain Res 1993, 20:209–220
19. Vidal M, Morris R, Grosveld F, Spanopoulou E: Tissue-specific control elements of the Thy-1 gene. EMBO J 1990, 9:833–840
20. Wirths O, Multhaup G, Czech C, Blanchard V, Tremp G, Pradier L, Beyreuther K, Bayer TA: Reelin in plaques of beta-amyloid precursor protein and presenilin-1 double-transgenic mice. Neurosci Lett 2001, 316:145–148
21. Hirrlinger PG, Scheller A, Braun C, Quintela-Schneider M, Fuss B, Hirrlinger J, Kirchhoff F: Expression of reef coral fluorescent proteins in the central nervous system of transgenic mice. Mol Cell Neurosci 2005, 30:291–303
22. Mailliot C, Sergeant N, Bussiere T, Caillet-Boudin ML, Delacourte A, Buee L: Phosphorylation of specific sets of tau isoforms reflects different neurofibrillary degeneration processes. FEBS Lett 1998, 433:201–204
23. Braak H, Braak E: Demonstration of amyloid deposits and neurofibrillary changes in whole brain sections. Brain Pathol 1991, 1:213–216
24. Irwin S: Comprehensive observational assessment: Ia. A systematic, quantitative procedure for assessing the behavioral and physiologic state of the mouse. Psychopharmacologia 1968, 13:222–257
25. Bliss TV, Collingridge GL: A synaptic model of memory: long-term potentiation in the hippocampus. Nature 1993, 361:31–39
26. Spittaels K, Van den Haute C, Van Dorpe J, Bruynseels K, Vandezande K, Laenen I, Geerts H, Mercken M, Sciot R, Van Lommel A, Loos R, Van Leuven F: Prominent axonopathy in the brain and spinal cord of transgenic mice overexpressing four-repeat human tau protein. Am J Pathol 1999, 155:2153–2165
27. Terwel D, Lasrado R, Snauwaert J, Vandeweert E, Van Haesendonck C, Borghgraef P, Van Leuven F: Changed conformation of mutant Tau-P301L underlies the moribund tauopathy, absent in progressive, nonlethal axonopathy of Tau-4R/2N transgenic mice. J Biol Chem 2005, 280:3963–3973
28. Ramsden M, Kotilinek L, Forster C, Paulson J, McGowan E, SantaCruz K, Guimaraes A, Yue M, Lewis J, Carlson G, Hutton M, Ashe KH: Age-dependent neurofibrillary tangle formation, neuron loss, and memory impairment in a mouse model of human tauopathy (P301L). J Neurosci 2005, 25:10637–10647
29. Sergeant N, David JP, Goedert M, Jakes R, Vermersch P, Buee L, Lefranc D, Wattez A, Delacourte A: Two-dimensional characterization of paired helical filament-tau from Alzheimer's disease: demonstration of an additional 74-kDa component and age-related biochemical modifications. J Neurochem 1997, 69:834–844
30. Lee G, Rook SL: Expression of tau protein in non-neuronal cells: microtubule binding and stabilization. J Cell Sci 1992, 102:227–237
31. Spillantini MG, Crowther RA, Kamphorst W, Heutink P, van Swieten JC: Tau pathology in two Dutch families with mutations in the microtubule-binding region of tau. Am J Pathol 1998, 153:1359–1363
32. Bronner IF, ter Meulen BC, Azmani A, Severijnen LA, Willemsen R, Kamphorst W, Ravid R, Heutink P, van Swieten JC: Hereditary Pick's disease with the G272V tau mutation shows predominant three-repeat tau pathology. Brain 2005, 128:2645–2653
33. Sperfeld AD, Collatz MB, Baier H, Palmbach M, Storch A, Schwarz J, Tatsch K, Reske S, Joosse M, Heutink P, Ludolph AC: FTDP-17: an early-onset phenotype with parkinsonism and epileptic seizures caused by a novel mutation. Ann Neurol 1999, 46:708–715
34. Probst A, Gotz J, Wiederhold KH, Tolnay M, Mistl C, Jaton AL, Hong M, Ishihara T, Lee VM, Trojanowski JQ, Jakes R, Crowther RA, Spillantini MG, Burki K, Goedert M: Axonopathy and amyotrophy in mice transgenic for human four-repeat tau protein. Acta Neuropathol (Berl) 2000, 99:469–481
35. Andorfer C, Acker CM, Kress Y, Hof PR, Duff K, Davies P: Cell-cycle reentry and cell death in transgenic mice expressing nonmutant human tau isoforms. J Neurosci 2005, 25:5446–5454
36. Zhang B, Higuchi M, Yoshiyama Y, Ishihara T, Forman MS, Martinez D, Joyce S, Trojanowski JQ, Lee VM: Retarded axonal transport of R406W mutant tau in transgenic mice with a neurodegenerative tauopathy. J Neurosci 2004, 24:4657–4667
37. Lim F, Hernandez F, Lucas JJ, Gomez-Ramos P, Moran MA, Avila J: FTDP-17 mutations in tau transgenic mice provoke lysosomal abnormalities and Tau filaments in forebrain. Mol Cell Neurosci 2001, 18:702–714
38. Bugiani O, Murrell JR, Giaccone G, Hasegawa M, Ghigo G, Tabaton M, Morbin M, Primavera A, Carella F, Solaro C, Grisoli M, Savoiardo M, Spillantini MG, Tagliavini F, Goedert M, Ghetti B: Frontotemporal dementia and corticobasal degeneration in a family with a P301S mutation in tau. J Neuropathol Exp Neurol 1999, 58:667–677
39. Lossos A, Reches A, Gal A, Newman JP, Soffer D, Gomori JM, Boher M, Ekstein D, Biran I, Meiner Z, Abramsky O, Rosenmann H: Frontotemporal dementia and parkinsonism with the P301S tau gene mutation in a Jewish family. J Neurol 2003, 250:733–740
40. Casseron W, Azulay JP, Guedj E, Gastaut JL, Pouget J: Familial autosomal dominant cortico-basal degeneration with the P301S mutation in the tau gene: an example of phenotype variability. J Neurol 2005, 252:1546–1548
41. Yasuda M, Nakamura Y, Kawamata T, Kaneyuki H, Maeda K, Komure O: Phenotypic heterogeneity within a new family with the MAPT p301s mutation. Ann Neurol 2005, 58:920–928
42. Buee L, Bussiere T, Buee-Scherrer V, Delacourte A, Hof PR: Tau protein isoforms, phosphorylation and role in neurodegenerative disorders. Brain Res Brain Res Rev 2000, 33:95–130
43. Arendt T, Stieler J, Strijkstra AM, Hut RA, Rudiger J, Van der Zee EA, Harkany T, Holzer M, Hartig W: Reversible paired helical filament-like phosphorylation of tau is an adaptive process associated with neuronal plasticity in hibernating animals. J Neurosci 2003, 23:6972–6981
44. Planel E, Miyasaka T, Launey T, Chui DH, Tanemura K, Sato S, Murayama O, Ishiguro K, Tatebayashi Y, Takashima A: Alterations in glucose metabolism induce hypothermia leading to tau hyperphosphorylation through differential inhibition of kinase and phosphatase activities: implications for Alzheimer's disease. J Neurosci 2004, 24:2401–2411
45. Sassin I, Schultz C, Thal DR, Rub U, Arai K, Braak E, Braak H: Evolution of Alzheimer's disease-related cytoskeletal changes in the basal nucleus of Meynert. Acta Neuropathol (Berl) 2000, 100:259–269
46. Sahara N, Lewis J, DeTure M, McGowan E, Dickson DW, Hutton M, Yen SH: Assembly of tau in transgenic animals expressing P301L tau:

alteration of phosphorylation and solubility. J Neurochem 2002, 83:1498–1508
47. Augustinack JC, Schneider A, Mandelkow EM, Hyman BT: Specific tau phosphorylation sites correlate with severity of neuronal cytopathology in Alzheimer's disease. Acta Neuropathol (Berl) 2002, 103:26–35
48. Bellucci A, Westwood AJ, Ingram E, Casamenti F, Goedert M, Spillantini MG: Induction of inflammatory mediators and microglial activation in mice transgenic for mutant human P301S tau protein. Am J Pathol 2004, 165:1643–1652
49. Blanchard V, Moussaoui S, Czech C, Touchet N, Bonici B, Planche M, Canton T, Jedidi I, Gohin M, Wirths O, Bayer TA, Langui D, Duyckaerts C, Tremp G, Pradier L: Time sequence of maturation of dystrophic neurites associated with Abeta deposits in APP/PS1 transgenic mice. Exp Neurol 2003, 184:247–263
50. Masliah E, Mallory M, Hansen L, DeTeresa R, Alford M, Terry R: Synaptic and neuritic alterations during the progression of Alzheimer's disease. Neurosci Lett 1994, 174:67–72
51. Chan SL, Furukawa K, Mattson MP: Presenilins and APP in neuritic and synaptic plasticity: implications for the pathogenesis of Alzheimer's disease. Neuromolecular Med 2002, 2:167–196
52. Pennanen L, Welzl H, D'Adamo P, Nitsch RM, Gotz J: Accelerated extinction of conditioned taste aversion in P301L tau transgenic mice. Neurobiol Dis 2004, 15:500–509
53. Decker MW, Curzon P, Brioni JD: Influence of separate and combined septal and amygdala lesions on memory, acoustic startle, anxiety, locomotor activity in rats. Neurobiol Learn Mem 1995, 64:156–168
54. Arriagada PV, Growdon JH, Hedley-Whyte ET, Hyman BT: Neurofibrillary tangles but not senile plaques parallel duration and severity of Alzheimer's disease. Neurology 1992, 42:631–639
55. Arendash GW, Lewis J, Leighty RE, McGowan E, Cracchiolo JR, Hutton M, Garcia MF: Multi-metric behavioral comparison of APPsw and P301L models for Alzheimer's disease: linkage of poorer cognitive performance to tau pathology in forebrain. Brain Res 2004, 1012:29–41
56. Braak H, Braak E: Neuropathological stageing of Alzheimer-related changes. Acta Neuropathol (Berl) 1991, 82:239–259
57. LaFerla FM, Oddo S: Alzheimer's disease: Abeta, tau and synaptic dysfunction. Trends Mol Med 2005, 11:170–176
58. Delacourte A, Sergeant N, Champain D, Wattez A, Maurage CA, Lebert F, Pasquier F, David JP: Nonoverlapping but synergetic tau and APP pathologies in sporadic Alzheimer's disease. Neurology 2002, 59:398–407
59. Gotz J, Chen F, van Dorpe J, Nitsch RM: Formation of neurofibrillary tangles in P301l tau transgenic mice induced by Abeta 42 fibrils. Science 2001, 293:1491–1495
60. Lewis J, Dickson DW, Lin WL, Chisholm L, Corral A, Jones G, Yen SH, Sahara N, Skipper L, Yager D, Eckman C, Hardy J, Hutton M, McGowan E: Enhanced neurofibrillary degeneration in transgenic mice expressing mutant tau and APP. Science 2001, 293:1487–1491
61. Bussiere T, Hof PR, Mailliot C, Brown CD, Caillet-Boudin ML, Perl DP, Buee L, Delacourte A: Phosphorylated serine422 on tau proteins is a pathological epitope found in several diseases with neurofibrillary degeneration. Acta Neuropathol (Berl) 1999, 97:221–230
62. Seubert P, Mawal-Dewan M, Barbour R, Jakes R, Goedert M, Johnson GV, Litersky JM, Schenk D, Lieberburg I, Trojanowski JQ, Lee VMY: Detection of phosphorylated Ser262 in fetal tau, adult tau, and paired helical filament tau. J Biol Chem 1995, 270:18917–18922
63. Oddo S, Caccamo A, Shepherd JD, Murphy MP, Golde TE, Kayed R, Metherate R, Mattson MP, Akbari Y, LaFerla FM: Triple-transgenic model of Alzheimer's disease with plaques and tangles: intracellular Abeta and synaptic dysfunction. Neuron 2003, 39:409–421
64. Fujimori F, Takahashi K, Uchida C, Uchida T: Mice lacking Pin1 develop normally, but are defective in entering cell cycle from G(0) arrest. Biochem Biophys Res Commun 1999, 265:658–663
65. Ahlijanian MK, Barrezueta NX, Williams RD, Jakowski A, Kowsz KP, McCarthy S, Coskran T, Carlo A, Seymour PA, Burkhardt JE, Nelson RB, McNeish JD: Hyperphosphorylated tau and neurofilament and cytoskeletal disruptions in mice overexpressing human p25, an activator of cdk5. Proc Natl Acad Sci USA 2000, 97:2910–2915